

IMPERIAL COLLEGE LONDON
DEPARTMENT OF PHYSICS

A Complexity Science Approach to Atrial Fibrillation

CMTH-Christensen-1

MSci REPORT

Author CID: 00695647

Assessor
Dr. Tim EVANS

Supervisor
Prof. Kim CHRISTENSEN

April 27, 2015

Abstract

Atrial fibrillation is the most common cardiac arrhythmia and a major cause of strokes. Despite this, the mechanics are still not fully understood. This project used a cellular automaton model, discretising the cardiac muscle cells to allow fast simulations and results. A square lattice model was built first, using ideas developed by Christensen et al. The model was then extended to a hexagonal lattice to better mimic the coupling of heart cells, in order to improve fidelity and measure new aspects. Further, heterogeneity of the conduction velocity was introduced in the model, based on the connectivity of the individual cell. Results were obtained in an identical fashion to the original model to allow direct comparison. Additionally, patches of irregular tissue were introduced into the model, initiating atrial fibrillation but not perpetuating it. This highlighted new, measurable features that could be studied further. Recognising critical structures as well as identifying and understanding causes based on characteristics seen during atrial fibrillation can aid its treatment in patients.

CONTENTS

1	Introduction	1
1.1	The Heart	1
1.1.1	Electrophysiology	1
1.1.2	Atrial Fibrillation	4
2	Theories of the Underlying Mechanisms	5
2.1	Ectopic Foci	5
2.2	Circus Movement Reentry	5
2.3	Multiple Wavelet Hypothesis	5
2.4	Leading Circle Hypothesis	6
2.5	Spiral Waves and the Mother Rotor Hypothesis	6
3	Treatment	7
4	Computer Modelling Atrial Fibrillation	8
4.1	Biophysical Models	8
4.2	Cellular Automaton Models	8
4.3	Christensen's Cellular Automaton Model	9
4.3.1	Risk of Atrial Fibrillation	10
5	Model Structure	12
5.1	Original Model	12
5.2	Extensions to Original Model	14
5.2.1	Hexagonal Lattice	14
5.2.2	Heterogeneous Conduction Velocity	16
5.2.3	Patches of Irregular Tissue	17
6	Results and Discussion	19
6.1	Errors	19
6.2	Hexagonal and Square Lattice	19
6.2.1	Visualisation	19
6.2.2	Risk of Fibrillation	20
6.3	Heterogeneous Conduction Velocity	21
6.3.1	Average Timedelay	23
6.3.2	Extremal Statistics	24
6.3.3	Weighted Timedelay	26
6.4	Risk of Fibrillation for All Models	28
6.5	Patches of Irregular Tissue	28
6.5.1	Reduced Local Transverse Coupling Probability	29
6.5.2	Connectivity at the Percolation Threshold	31
6.5.3	Comparison of Both Models	32
7	Conclusions and Future Study	34
8	Acknowledgements	35
A	Derivation of the Risk of Atrial Fibrillation	39
A.1	Homogeneous Conduction Velocity	39
B	Computational Code	40

SUMMARY

Atrial fibrillation is a heart condition and a major cause of strokes. This project aims to further understand mechanisms within the heart during atrial fibrillation by producing a simple computer model that discretises the heart cells. This type of computer program is called a cellular automaton model. The project extended previous work by Christensen and Manani, improving the fidelity of the original model by increasing its complexity.

Section 1 introduces atrial fibrillation and provides an overview of the importance of the work being undertaken. The normal function of the heart is described, its electrophysiology and function during atrial fibrillation. In particular, how conduction is passed cell to cell and the coupling structure of heart cells.

Section 2 examines current and past theories surrounding the mechanics of atrial fibrillation that have been explored for over a century. The two main theories, ectopic foci and circus movement reentry are described. Subsequent theories extending from these are also discussed.

Section 3 describes current treatment methods used for atrial fibrillation. With better understanding of the full mechanics, critical regions may be more easily identified which would lead to more effective treatment.

Section 4 reviews different forms of computational programs that have been developed. These include realistic biophysical models, which describe the transportation of ions between heart cells causing conduction. Other models include cellular automata. The basis for this project, Christensen *et al*'s cellular automaton model is described and the parameters involved. The risk of fibrillation is quantified as a probability which was developed by Christensen *et al*. This square lattice model is extended further to a hexagonal lattice to fit with the model later implemented.

Section 5 describes the model's implementation, including the original square lattice algorithm structure (written in C++) and visualisation methods used. It further explains extensions to the original model. These include the shift to a hexagonal lattice and the introduction of heterogeneous conduction velocity and irregular patches of tissue within the heart.

Section 6 presents the results obtained and discusses these findings. This includes verification of the previous model with regards to the risk of fibrillation and findings with the extensions described.

Section 7 concludes the findings of this project and describes possible further work.

DECLARATION

The computational program was built upon the ideas and parameters from the original model put forth by the project supervisor Professor Kim Christensen and PhD student Kishan Manani. The computational model was created solely by the author and the project partner, with a joint effort to implement the initial model.

The extensions to the model were discussed with the supervisor and PhD student and used their guidance. Methods of physically implementing new features were discussed between the author and the project partner. The code was written largely together with both parts offering knowledge and insight into physically modelling sections and making these run more efficiently.

The program was written in C++ with analysis undertaken using Excel and final results presented using Origin Pro. Results and analysis were done separately with equal split between work. For example, the author developed the results for the patch at the percolation threshold (section 6.5.2) while the partner developed results for the patch with lower local transverse connectivity (section 6.5.1).

1 INTRODUCTION

Atrial fibrillation (AF) is the most common cardiac arrhythmia and the instigating factor for many chronic heart conditions. It is also the most significant cause of ischaemic stroke in older age groups [1]. Instead of contracting normally, the heart undergoes 400-600 bpm and is irregular, prohibiting the heart's efficient contraction. Despite over 100 years of study, the full mechanics of AF are not understood [1]. Due to an ageing population, it is likely that the number affected by AF will dramatically increase. It is therefore ever more important to find better techniques for locating atrial areas that are significant in the initiation of AF.

There has been some success in medical treatments, particularly with ablation techniques [2, 3]. However, it is thought that improved methods of finding localised sources could make treatments more effective [2]. A better understanding of characteristics that arise may make it possible to pinpoint critical regions , through the use of computational simulations. Ethical problems in animal studies as well as the difficulty in accurately mapping AF-related sources and wavelets in human studies, make computer models an attractive alternative [4]. This project aims to build a computer simulation, extending previous work of Christensen *et al* [40], modelling AF in order to further understand arising complex behaviour. Improved understanding of the mechanics will aid better treatment in patients. This work is therefore of vital importance.

1.1 THE HEART

1.1.1 ELECTROPHYSIOLOGY

The heart consists of four chambers: two ventricles and two atria (see figure 1). It comprises discrete, excitable cardiac muscle cells (cardiomyocytes), which contract upon excitation. The cells of the sinoatrial node (SAN) act as the system's natural pacemaker undergoing regular depolarisation and repolarisation [5]. This is the result of a careful transport of ions through the cell membrane via gap junctions and causes a change in the potential difference between the inside and outside of a cell - this is called the action potential (AP) [6]. The gap junctions form the coupling structure of cardiomyocytes, allowing the propagation of APs between cells [7]. These APs force blood from the atria to enter the ventricles, which is then pushed around the rest of the body. In a healthy heart, cardiomyocytes experience synchronised contraction, resulting in efficient pumping of blood.

ACTION POTENTIALS

The AP is the voltage variation that the cardiomyocytes undergo with time. This is controlled by the transfer of ions through cell membrane, specifically Na^+ , K^+ and Ca^{2+} ions (see figure 2). During the first phase of the AP, the cell rapidly depolarises due to a net flow of positive ions entering the cell, causing a sharp rise in its potential. After a plateau, the cell undergoes a final repolarisation where a net flow of positive ions leave the cell. Once the cell reaches a resting state, called the threshold potential, it is excitable once more. Certain states of refractoriness may be excitable, however not easily. This process typically lasts around 150ms.

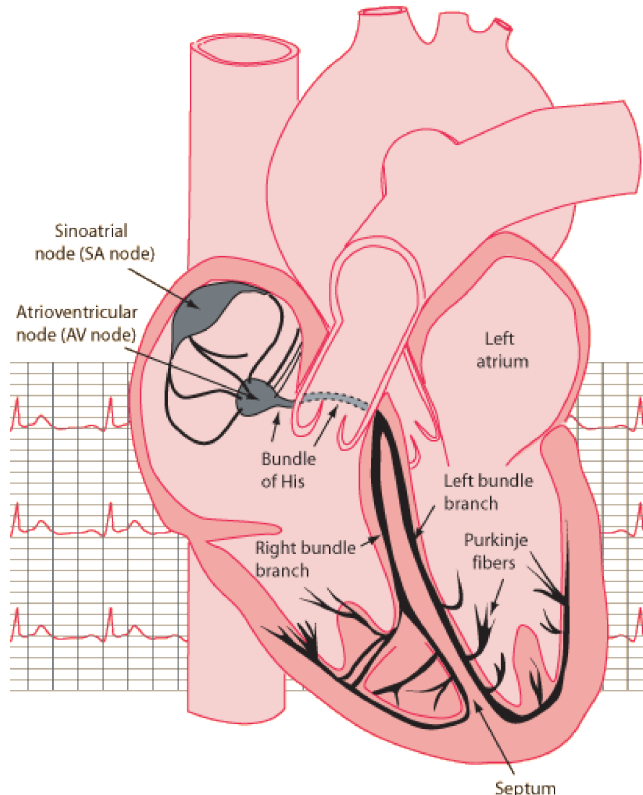


Figure 1: *The Heart* [5]. Cells of the SAN can be seen in the right atrium. These fire at regular intervals, controlling automaticity.

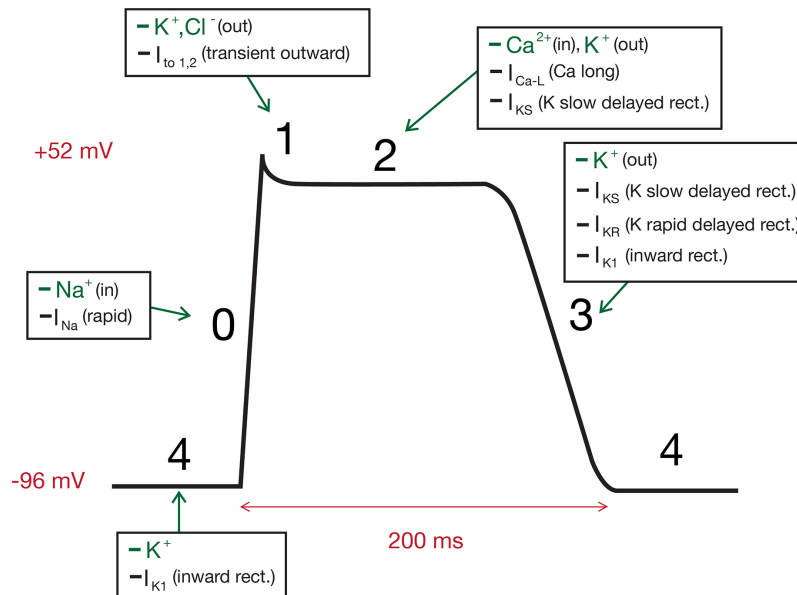


Figure 2: *The Action Potential* [8]. The voltage-time dependence of a cell during excitation. The cell undergoes rapid depolarisation during phase 0, shown by the sharp rise in its potential. The potential plateaus (phase 2) before repolarising (phase 3), shown by the downward slope. When the cell reaches the resting potential (phase 4), it is excitable again.

CELL-CELL COUPLING AND WAVEFRONT PROPAGATION

The branching cell structure of the myocardium (cardiac muscle) is shown in figure 3. Cardiomyocytes of the atria are predominantly coupled in the longitudinal direction, but possess many transverse neighbours. There is evidence to suggest the number of transverse connections is inversely related to age [9].

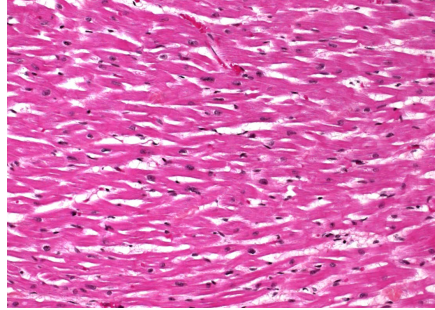


Figure 3: *Cardiac Cells of the Myocardium* [10].

The conduction velocity in the transverse direction, Θ_T is known to be slower than conduction in the longitudinal direction, Θ_L . Evidence suggests there is a decoupling of cells in the transverse direction with older age groups [9]. This is supported by observations that the fraction Θ_L/Θ_T increases with older age groups, due to an increase in Θ_L as well as a decrease in Θ_T . The sparser nature of transverse connections because of the decoupling of cells would cause a decrease in Θ_T due to the extended path the wavefront must undergo [9, 11]. This, combined with lowering resistivity in the longitudinal direction supports these findings [9, 12].

The number of connections an individual cell possesses may also affect wavefront propagation. Spector [13] described a bucket analogy to explain a source-sink mismatch between a cell and the number of links it possesses. The source of a cell is the electrical charge it receives by its neighbours, the sink is the charge it gives out. The more holes a bucket has, the longer filling it with electrical charge takes until the excitation threshold is reached, because the holes contribute to its sink. A bucket with more holes is analogous to a cell with more couples. A cell with more couples has a reduced source-sink ratio and therefore passes conduction slower. This is shown schematically in figure 4.

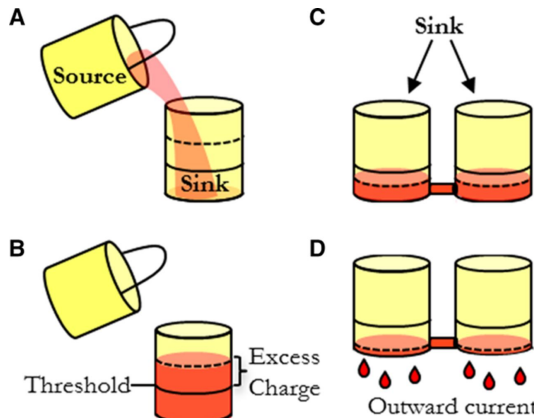


Figure 4: *Source-Sink Bucket Analogy* [13]. **A** a cell providing charge (source) to another cell (sink) until it passes excitation threshold **B** at which point the cell may fire. **C** a sink with more holes (couples) takes longer to reach excitation threshold because of the increase in its sink, passing conduction slower.

1.1.2 ATRIAL FIBRILLATION

AF is characterised by the abnormal disruption of regular heart rhythm, originating in the atria. During regular cardiac rhythm, the heart rate is around 60 bpm. During AF, it may reach 400-600 pulses and pumps inefficiently due to chaotic currents on the surface of the myocardium [1]. Although the mechanics are not fully understood, it is thought that a reentrant arrhythmia and a number of other factors contribute to the perpetuation of AF [14, 15]. AF can be described by different classes. Paroxysmal AF describes episodes that are intermittent, typically lasting less than 7 days. Persistent AF applies to episodes lasting longer than 7 days and are continual [16].

2 THEORIES OF THE UNDERLYING MECHANISMS

There were two main theories surrounding the mechanics of AF that dominated the first half of the 20th century - ectopic foci and circus movement reentry, with experimental evidence supporting both hypotheses [2, 17, 18]. There have been extensions and variations of both.

2.1 ECTOPIC FOCI

The ectopic foci theory supposes that AF is the consequence of a rapidly discharging source(s), causing the cardiac impulses to become chaotic. The theory was first introduced by Winterberg [19] in 1907 and confirmed experimentally by Scherf *et al* [20] in 1948, by inducing tachycardia in canine hearts. Scherf noted that cooling the atria should cause complete arrest of the tachycardia if circus movement reentry was the cause. Instead, he found that it returned upon removal of the cooling device and deduced that an ectopic focus must be the stimulus. Ectopic foci have also been found more recently in human studies and were largely the result of single stimuli [2].

2.2 CIRCUS MOVEMENT REENTRY

In 1913, Mines [21] progressed the circus movement reentry theory. If a cell is excited within a closed circuit and the speed of propagation is slow compared with the duration, it is possible that cells have time to return to an excitable state and can therefore be re-excited by the time the wave completes the circuit. This is shown schematically in figure 5. Experimental evidence was shown for circus movements by Rosenblueth *et al* [18] - waves in canine hearts circulating a fixed path.

2.3 MULTIPLE WAVELET HYPOTHESIS

In 1959, Moe and Abildskov [22] presented the Multiple Wavelet hypothesis, explaining the chaotic nature of fibrillation. They describe a wavefront fractionating into multiple daughter wavelets and stress that the initiating factor could be due to an ectopic focus *or* a circus movement. The probability that fibrillation is sustained depends on the number of multiple wavelets present. The larger the value, the more likely that at least one will survive. Experimental evidence of these wave types in canine hearts have been shown to exist during AF [23]. Two factors favouring a large number of wavelets are the mass of the atria and the brevity of the refractory period, independent of the initiator. In general, it is thought that this is the cause of persistent AF [15].



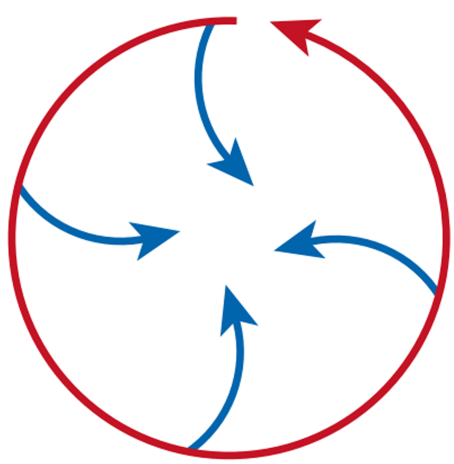
Figure 5: *Circus Movement Reentry* [21]. In this closed circuit, the wavefront is represented by excited cells shown in black and those in the refractory period are shown as dots. Reentry is shown to be sustained.

2.4 LEADING CIRCLE HYPOTHESIS

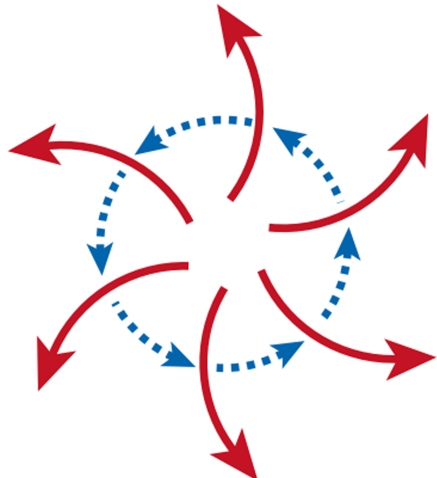
Allessie *et al* [24] developed the Leading Circle hypothesis, introducing the concept of the wavelength of reentry. The Leading Circle concept, an extension to circus movement reentry, describes the smallest possible circuit in which an impulse may be sustained, see figure 6a. A wavefront circulating tissue smaller than this would find itself attempting to excite refractory cardiomyocytes. The circuit pathlength (perimeter) must therefore be greater than or equal to the distance the impulse travels in one refractory period - the wavelength of reentry - for the wave to be sustained. The wavelength of reentry is the product of the impulse conduction velocity and the refractory period. An important outcome of this concept was that a circus movement does not necessarily form around a region of inexcitability, such as scar tissue. Treatment, thus has been to lengthen the refractory period, thereby increasing the wavelength of reentry. This increases the minimum pathlength of a reentrant wave, allowing fewer circuits within a fixed area of myocardium and decreasing the probability at least one will survive.

2.5 SPIRAL WAVES AND THE MOTHER ROTOR HYPOTHESIS

A rotor is a central core that drives reentrance, from which spiral waves may emanate (see figure 6b) [25]. Schuessler *et al* [14] induced tachycardia in canine hearts and found differing results to predictions by Moe [26]. Although sustained AF exhibited multiple reentry circuits, these were generally unstable. A dominant circuit would emerge, causing arrest of others [14]. This gave rise to the mother rotor hypothesis, which describes a dominant rotor - the source of the chaotic reentrant waves that arise in AF [27]. Schuessler *et al*'s findings pointed towards a single reentrant source - either a circus movement or an ectopic focus. There have since been multiple experiments conducted supporting this theory [15, 27, 28, 29, 30, 31].



(a) *Leading Circle Hypothesis* [1]



(b) *A Spiral Wave* [1]

Figure 6: (a) The leading circle hypothesis describes the smallest circuit by which an impulse may travel and still be self sustaining [24]. (b) Spiral waves emanating from a rotor formed of an unexcited (but excitable) core.

3 TREATMENT

Treatments of AF include antiarrhythmic drugs and ablation techniques. Antiarrhythmic drugs aim to lengthen the refractory periods of cells, thereby increasing the wavelength of reentry and allowing fewer waves to propagate. Ablation techniques aim to remove sources of reentry. One successful ablation technique is the Maze procedure, whereby incisions in the heart are used to segment the atria, thus allowing very few wavelets to propagate [3].

With the exact causes for the initiation of AF unclear, it can be difficult to pinpoint critical areas of tissue for ablation techniques to be most effective [15]. The longevity of lifetimes of the daughter wavelets that arise from fractionation of spiral waves may lead to driving rotors unconnected to initiators [28]. This is supported by evidence that the initiating rotor often died during an AF episode [32]. Thus, wavelet patterns may misrepresent the underlying cause, and ablation techniques are ineffective at terminating persistent AF [32].

Catheter ablation has however seen success in patients where ectopic foci were the initiating event - one study showed 62% of ectopic focus cases found success with ablation after discharge from hospital [2]. It is thought that this success rate would increase if recognition and location of ectopic foci were improved. This may be achieved via computational simulations.

4 COMPUTER MODELLING ATRIAL FIBRILLATION

4.1 BIOPHYSICAL MODELS

Biophysical models describe the heart on a subcellular level in a continuous medium, allowing a realistic and accurate representation. They include features such as ion exchange and current flow across cell membrane, often resulting in lengthy and complex partial differential equations (PDEs) that are costly to solve [4, 33]. An example of such a model includes one built by Ruchat *et al* in 2007 [34].

4.2 CELLULAR AUTOMATON MODELS

Cellular automaton (CA) models aim to simplify the myocardium by using a dynamical system of discrete cells, each of which may take on a discrete state dependent on the states of their neighbours. States may change at each timestep [33, 35]. The advantages of using CA models include simplicity, and a lack of need for PDEs while still displaying complex behaviour [35].

There have since been many variations of CA models, all of which follow the same basic structure [36]. Each cell may be in the resting, refractory or excited states [26, 37]. A cell may become excited in the next timestep when one of its nearest neighbours is excited, provided the cell is in an excitable state.

Moe *et al* [26] built one of the first 2D computer simulations modelling AF, using a CA model with discrete hexagonal cardiomyocytes in a heterogeneous spread of refractoriness. The model generated reentry circuits, without the need for an anatomical obstacle (region of inexcitability), due to this non-uniformity. Elongating the refractory period and building a smaller system reduced the probability that AF was maintained, as previously predicted [22].

Other models have made variations to highlight the effect of different aspects. Gerhardt *et al* [33] included the effects of curvature and dispersion. Spiral waves showed spontaneous wave breakup, occurring in a spatially uniform medium, and generated daughter wavelets. Bub *et al* [38, 39] built on previous work by Greenberg and Hastings [37], and introduced spatial heterogeneity by varying the cell density. Spatially organised “bursting rotors” were observed when cell density was reduced. This spatiotemporal organisation was similar to findings by Jalife and his laboratory [28].

Reumann *et al* [32] extended the CA model to 3D by modelling an anatomically realistic heart. Ectopic foci were built into the pulmonary veins in the simulation because of evidence in recent studies suggesting the likelihood of formation here [27]. The self-termination of initiating rotors gave rise to deceptive patterns of wavelet propagation, making it difficult to determine the location of the reentrant source.

4.3 CHRISTENSEN'S CELLULAR AUTOMATON MODEL

Christensen *et al* [40] built a CA model introducing heterogeneity by using a control parameter, coupling cells vertically with a given probability ν - replicating the branching structure of the myocardium. A square lattice with all cells connected horizontally was implanted. The probability of defective cells was fixed, $\delta = 5\%$ and had a probability of dysfunction, $\epsilon = 5\%$ while the control parameter was altered across simulations. Figure 7 shows these features schematically. A resting cell will excite in the following timestep if a (coupled) neighbour is excited, giving a conduction velocity (CV) of one timestep.

It was found that below a particular threshold, $\nu^* \approx 0.14$, the system entered into a fibrillatory state. Above this however, a sharp (phase) transition appeared and plane waves propagated through the myocardium. These findings are consistent with evidence that transverse coupling is affected by age. The decoupling of cells in the transverse direction as patients age is followed with an increased prominence of AF, as demonstrated in this study.

FIXED PARAMETERS

The lattice was set up by coarse graining typical parameters found for a physical heart using a scale factor of $b = 5$. Atrial tissue in a heart has an area of $\approx 20\text{cm}^2$. Dividing by the cell lengths in the longitudinal, $\Delta x' \approx 100\mu\text{m}$ and transverse direction, $\Delta y' \approx 20\mu\text{m}$ gives the number of cells in the lattice, $L \times L = 10^6$ cells. Using the scale factor b , the new lattice length scale becomes $L = 200$ cells where each individual cell represents $b \times b$ cells in real tissue. The conduction velocity in this model is given as 1 cell per timestep for simplicity and is representative of the timescale for a cell to depolarise, $\Delta t' \approx 0.6\text{ms}$. In physical terms, this becomes $\Delta t' \rightarrow b\Delta t'$ due to the scale factor. Dividing through typical values found for the refractory period, $\tau' = 150\text{ms}$ by this gives the refractory period in this model, $\tau = 50$ timesteps. The SAN was modelled via the excitation of cells in the left-most column at a fixed period (SAP) of $T = 220$ timesteps. As stated previously, this initialises the wavefront that propagates across the atria, causing the pumping action. A summary of the parameters used is given in table 1. [40]

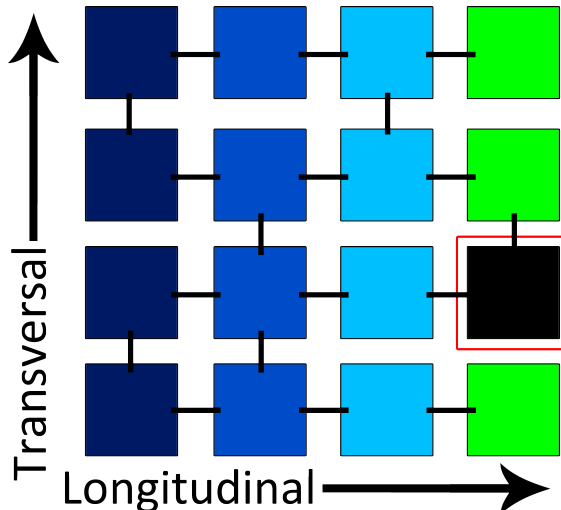


Figure 7: *Basic CA Model.* The coupling of cells allows for the propagation of wavefronts. Excited cells are indicated by green, the resting state is black, refractory states are shown in blue fading to black. The defective cell is shown with a red box and has failed to be excited by its neighbours.

Characteristic	Symbol	Value
Lattice length	L	200 cells
Sinal Atrial Node Period (SAP)	T	220 timesteps
Refractory period	τ	50 timesteps
Probability of defective cells	δ	5%
Probability of dysfunction	ϵ	5%
Probability of transverse coupling	ν	$0 \leq \nu \leq 1$

Table 1: *Parameters utilised for the CA model [40]*

The lattice was constructed to have periodic boundaries for the top and bottom rows. For example, cells residing in either of these rows may be connected if there existed a transverse connection. Thus forming cylindrical topology.

4.3.1 RISK OF ATRIAL FIBRILLATION

The risk of entering AF can be quantified by describing the probability that the system will enter into a fibrillatory state, P_{risk} . This section will quantify this probability, developed by Christensen *et al* [40] for a square lattice and will be extended to a hexagonal lattice for the context of this project.

Previously mentioned were the notions of rotors and the smallest possible circuit which allows reentry to occur, the wavelength λ . This is given by,

$$\lambda = CV \times \tau \quad (4.1)$$

Simplifying for the context of the model described here, where CV is one timestep:

$$\lambda = \tau \quad (4.2)$$

Reentry is facilitated in this model via defective cells and the frequency of transverse couplings. A critical region is defined as an area of tissue which may allow reentry to occur. In this model, this could appear at a defective cell in the event that it fails to fire. For this area to be considered critical, the path a wavefront will travel must be at least the size of the wavelength. This translates into the model by describing the distance between a defective cell and the first vertical couple to its right, l_i which must be $< \lambda/2$ in order to be non-critical. The $1/2$ arises so that when the wavefront turns back, the total path length will be $< \lambda$. This is shown schematically in figure 8 where for simplicity, $\tau = 5$.

Summing over all probabilities where the distance between a defective cell and its first transverse couple is less than $\lambda/2$, gives the probability that a defective cell is non-critical. Accounting for all defective cells in the lattice, gives the probability that all defective cells are non-critical. The risk of fibrillation, is characterised by the probability that at least one critical region will exist.

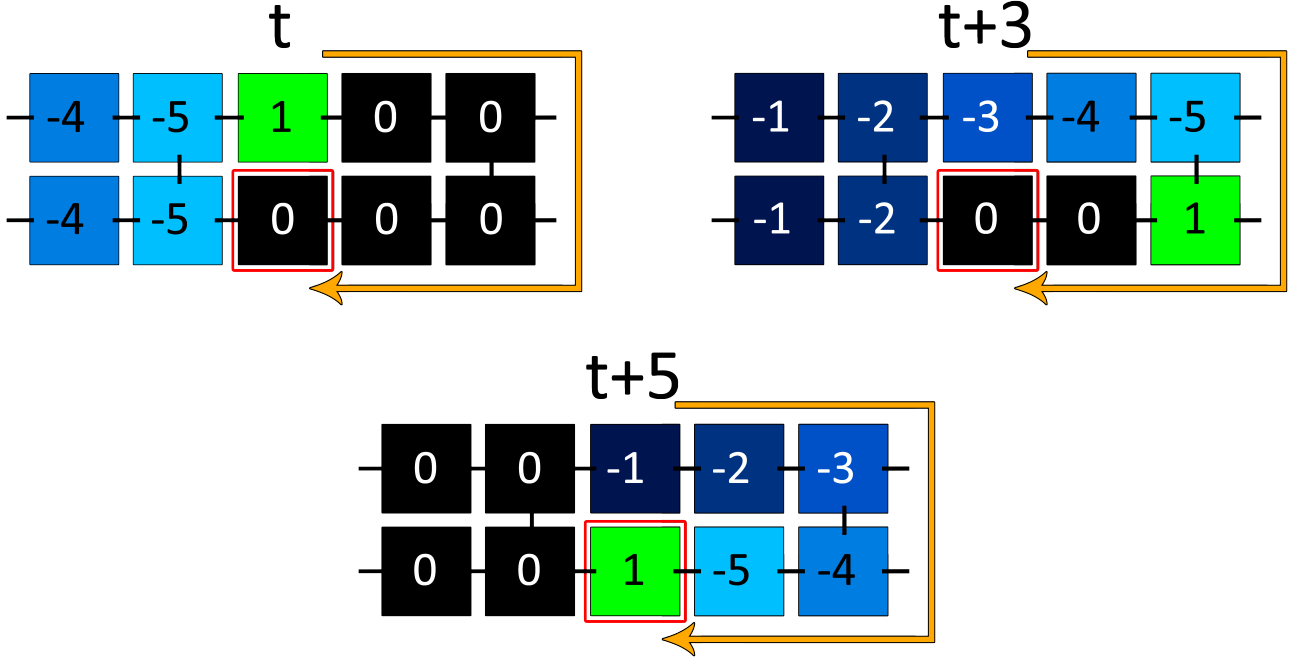


Figure 8: *Critical Regions*. A critical region appearing near a defective cell. Numbers within cells represent states. For example, 0 for refractory and 1 for excited. In the first image, the defective cell fails to excite by the excitation of its neighbours. The distance this wavefront travels in circulating back towards the defective cell (which is resting and excitable) is long enough to allow for the cell to its left to be excitable once more and so reentry occurs.

This becomes:

$$P_{\text{risk}} = 1 - \underbrace{\left[1 - (1 - p_\nu)^{\frac{\lambda}{2}} \right]^{\delta L^2}}_{\text{Prob. single defective cell is non-critical}} \quad (4.3)$$

Prob. all defective cells are non-critical

Where p_ν is the probability that any given cell has at least one transverse couple.

In the homogeneous model described here, $\lambda = \tau$ (see equation 4.1). The only parameter that differs between a hexagonal and a square lattice is p_ν , inputting separate equations for this probability gives P_{risk} for both of these lattices.

For a square lattice,

$$P_{\text{risk,square}} = 1 - [1 - (1 - \nu)^\tau]^{\delta L^2} \quad (4.4)$$

For a Hexagonal lattice,

$$P_{\text{risk,hex}} = 1 - [1 - (1 - \nu)^{2\tau}]^{\delta L^2} \quad (4.5)$$

For the full derivation of P_{risk} , please see appendix A.

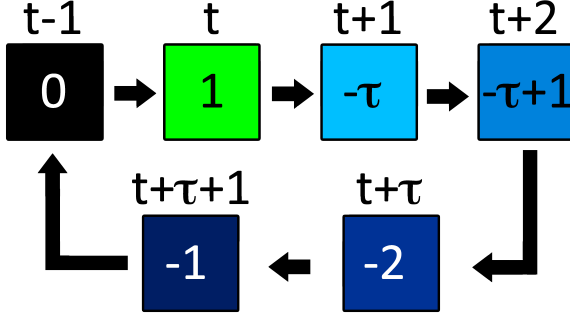
5 MODEL STRUCTURE

5.1 ORIGINAL MODEL

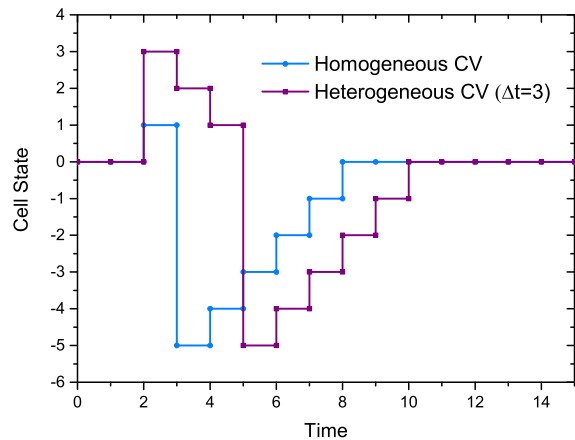
The model was constructed in C++ using Visual Studio 2013. The first step in writing the code was the initialisation of the lattice. This was implemented by defining a set of arrays describing the characteristics of individual cells. One-dimensional arrays representing individual cells could easily be mapped to their position. An array describing the coupling of the cardiomyocytes assigned every cell with a horizontal couple to its right, transverse couples were assigned using the Mersenne Twister random number generator for the given value of ν . Transverse couples were described in a downwards direction. A cell assigned with a transverse connection was considered to be coupled with the cell directly below it. Another array described whether cells were defective or not, assigned with probability δ . During a simulation, if a defective cell failed to fire when excited by a coupled cell, this particular cell was not given another chance to be excited again. Data for all simulations was taken over 50 seeds of the number generator and averaged across all. This was then analysed using Microsoft Excel and presented using Origin Pro.

CELL STATES

The discretisation of cell states is shown in figure 9. Values were given to cells representing specific states. For example, a resting cell had a state 0; excited cells had state 1; refractory cells were given a value of $-\tau$ and incremented each timestep until reaching the resting state once more. The SAN cells were a special case within the model, and modelled as though having their own refractory period of $T = 220$ timesteps. After being excited, their state would become $T + 1$ and decrement over time until reaching 1, exciting again. These cells therefore never entered the resting state and always excited with a fixed period.



(a) Progression of Cell States with Time



(b) Discretised Cell States

Figure 9: Demonstrating the state of a cell as time progresses. (a) The cell excites at time t and spends τ timesteps in the refractory state. The labels within the cell show the value of the discretised state given in the computational model. (b) Discretisation of cell states for both a homogeneous CV model and an example heterogeneous CV model - which will be discussed later. The refractory period in (b) is 5 for simplicity.

BASIC ALGORITHM STRUCTURE

The basic algorithm is as follows:

1. Initialisation

- (a) Declare arrays containing states of cells for the current and next timestep
- (b) Randomly choose defective cells with a probability δ
- (c) Randomly assign transverse couples with probability ν
- (d) Excite SAN cells (leftmost column)

2. Increment time

3. Scan through every cell within lattice, check state of cells

- (a) If cell is excited:
Set state of cell in next timestep to $-\tau$ or $T + 1$ if SAN cell
If a coupled cell is resting and not defective, excite in next timestep
If coupled cells are defective and resting, excite with probability $1 - \delta$
- (b) If cell is in refractory stage:
If SAN cell, decrement state in next timestep
All other elements, increment state in next timestep.

4. Return to 2

Repeat for 10^6 timesteps

Only conditions for excited or refractory cells were written for this process, resting cells were immediately ignored and the lattice loop moved onto the next cell. Every cell was checked and so an excited cell will always excite its resting neighbours. The majority of cells at any given moment were resting or refractory. Since refractory cells only needed a simple update of their state for the following timestep, this improved the efficiency of the program.

VISUALISATION

After the construction of the basic model, it was important to check correct behaviour was being displayed. This was implemented via the use of visualisation tools. The SFML library was used in displaying model behaviour throughout time increments. Excited cells were displayed in green, while refractory states were blue and faded to black as they entered stages closer to the resting state. Resting defective cells were shown in red, while all other resting states were shown in black. In order to make the visualisation tool run more efficiently, the basic window displayed was black and only cells that were either excited or refractory were drawn in each timestep.

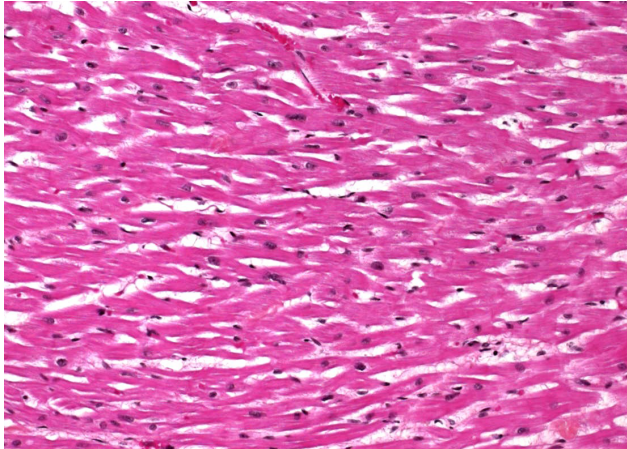
RISK OF ATRIAL FIBRILLATION

In determining whether the system entered AF, during every timestep the number of excited cells present for the following timestep were counted. If this number exceeded a particular threshold, the system was determined to be in AF for that timestep. Counting all the timesteps the system was in AF for, and dividing by the total time gave the percentage of time spent in AF - P_{risk} . The threshold determined was $1.2 \times L$, to account for L cells excited by the SAN and for small reentrant circuits that do not necessarily develop into AF.

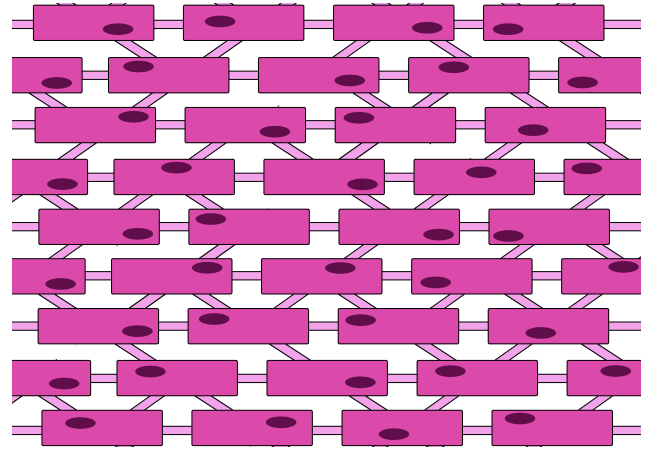
5.2 EXTENSIONS TO ORIGINAL MODEL

5.2.1 HEXAGONAL LATTICE

The model was extended to a hexagonal lattice to mimic more realistically the coupling structure of cardiomyocytes.



(a) *Real Cardiomyocytes* [10]



(b) *Cardiomyocytes as a Brick-Like Structure*

Figure 10: Representation of real cardiomyocytes as a brick-like structure. On average, cardiomyocytes will have more transverse neighbours than the two given for the square lattice. In a brick pattern, cells have four transverse neighbours and can be modelled easily using a hexagonal lattice.

Coupling of cardiomyocytes closely resembles more a brick-like structure with a maximum of four transverse connections versus the square lattice's two. Saffitz *et al* [11] found myocytes of the crista terminalis in the right atrium of canine hearts had 6.4 ± 1.7 connections which is closer to the 6 couples of the hexagonal model. It should be noted, cells do not serve to be a realistic representation and are used simply to model the coupling structure with more fidelity.

In building this model, mapping functions to a given cell's position by row and column were calculated. Special care and attention was required since the physical positions of a cell's neighbours were dependent on whether that particular cell resided in an even or odd row. The mapping functions used to find a cell's neighbours are shown in figure 11. Simple functions were written to map a given cell to its neighbours depending on whether it lay in an even or an odd row. This shortened the code significantly since separate conditions were not needed every time a cell's neighbours were required.

Other conditions needed to be considered. Such as, a cell residing in the last column on an odd row cannot physically possess right-diagonal couples due to the way in which the lattice was defined. Figure 12 demonstrates this more clearly.

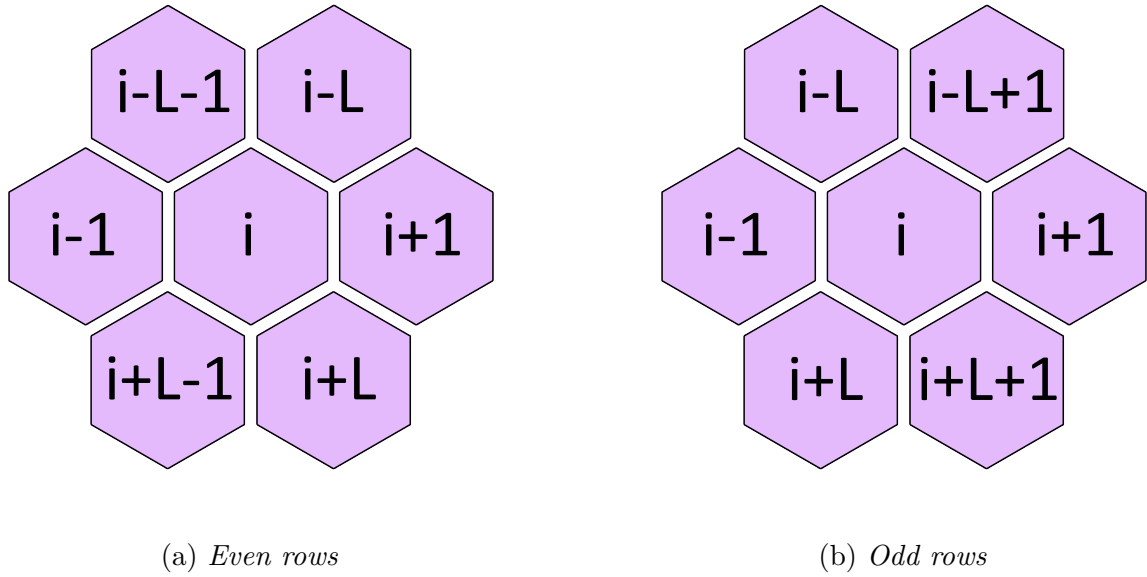


Figure 11: Mapping of a cell, i to its neighbours for both even and odd rows

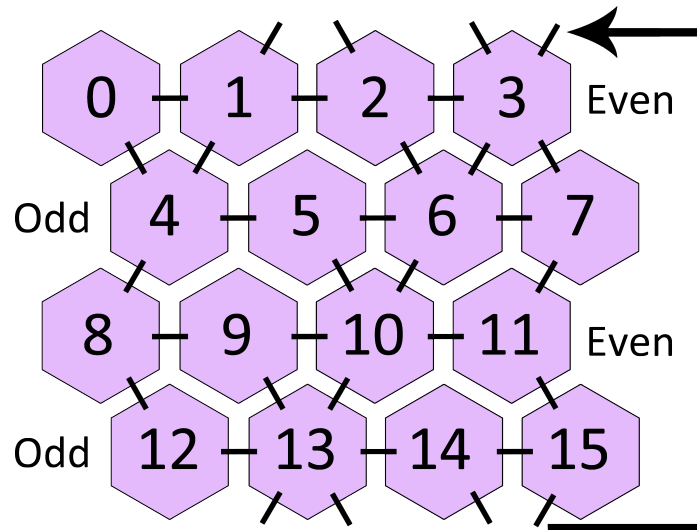


Figure 12: *Hexagonal Lattice Structure*. A lattice with dimensions $L \times L = 4$, directly equivalent to the way in which the $L \times L = 200$ lattice was constructed. The values within the cells represent the index each corresponds to within the equivalent arrays. Indexing always starts with the value 0, hence why the first row is considered to be even. Cells residing in the last column on an odd row do not have right diagonal neighbours. This was taken into account when assigning couples for a given ν . The arrow represents the periodic boundaries given to the first and last rows.

5.2.2 HETEROGENEOUS CONDUCTION VELOCITY

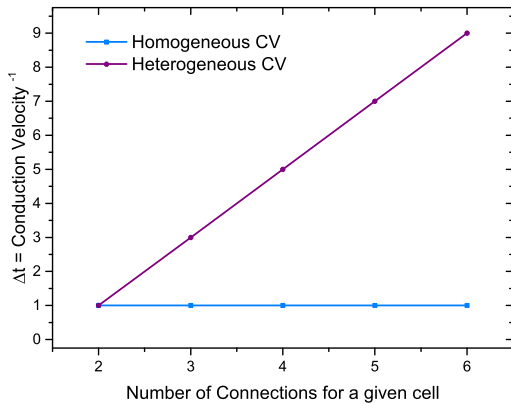
The original model was further extended to introduce heterogeneity for the CV of cells. This was implemented via a delay in excitation based on the number of couples an individual cell had. Due to the source-sink theory mentioned in section 1.1.1, cells with more couples had a greater timedelay - and effectively a slower CV - than those with fewer. A cell with two horizontal couples always had $CV = 1$ and therefore excited in the next timestep. For every extra transverse couple, a user-defined factor could be chosen to increment its timedelay by. For the results that follow, a factor of 2 was chosen. Therefore, a cell with the maximum number of connections (6 for a hexagonal lattice) had a timedelay of 9. Figure 13 demonstrates the timedelay given to a cell for every possible number of couples versus the previous model.

The CV of an individual cell can be derived simply from its timedelay, $\Delta t(\nu)$.

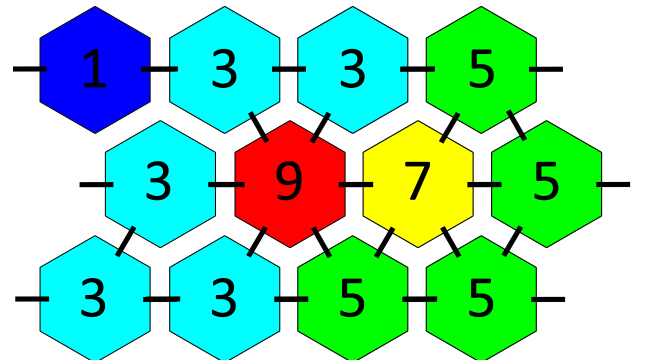
$$CV = [\Delta t(\nu)]^{-1} \quad (5.1)$$

It should be noted that these values were not based on true values found for CV, and is a simplification. The source-sink idea where CV of an individual is related to how many couples it possess, has been used for this model. It has also been observed that transverse CV is slower than longitudinal CV. The simplification with regards to this, is that a cell with any transverse connections instantly passes conduction slower (in the longitudinal direction as well as transverse). Even though individual cell conduction has been reduced in both directions, overall conduction is still faster in the longitudinal direction due to the straight path the wavefront travels in this case versus the zigzag path dependent on transverse cell connectivity.

This model is consistent with findings that the fraction Θ_L/Θ_T increases with older age groups [9, 12]. To serve as a reminder, a decrease in transverse connectivity (given by ν) has been linked to increasing age and the overall CV in this model increases for this case. This will be observed most prominently in the longitudinal direction since transverse connectivity is low. Conduction in the transverse direction will decrease as ν decreases simply due to the scarcity of transverse connections and is not observed on a cell-cell basis. Both these effects cause an increase in Θ_L/Θ_T , in agreement with findings in the ageing of patients.



(a) Number of Connections Vs Timedelay



(b) Visual Example with a Heat Gradient

Figure 13: Timedelays given to a cell with a varying number of couples. For every extra (transverse) couple given to a cell, its timedelay is incremented by 2 timesteps. The blue line in figure (a) represents the timedelay for the previous model, where CV was homogeneous and chosen to be 1 timestep.

Several alterations were made to account for CV slowing down for greater values of ν . The SAP previously allowed for at most one wavefront propagating through the lattice at any given moment. This had to be made true for any given value of ν to discourage false counting of time spent in AF. The SAP was such made dependent on the average timedelay across all cells for a given lattice.

$$SAP = \langle \Delta t \rangle \times 220 \quad (5.2)$$

Also, in order for fair simulations across the entire range, a fixed number of wavefronts initialised by the SAP were allowed for every given ν . Thus, the time loop length was redefined to directly depend on the average timedelay.

$$t_{\max} = \langle \Delta t \rangle \times t_{\max, \text{base}} \quad (5.3)$$

Previously, the simulation time was $t_{\max, \text{base}} = 10^6$ timesteps. For the most extreme case, $\nu = 1$ previously would have a simulation time of 9×10^6 timesteps. This was far to large to feasibly run and so $t_{\max, \text{base}}$ was reduced to 10^5 timesteps.

Previously, because $t_{\max, \text{base}} = 10^6$ was large, the time to change from transient to recurrent states was dwarfed in comparison to total time and so discount times were not considered. In this new model, the first 40 SAPs were ignored to allow for this change-over in simulations.

5.2.3 PATCHES OF IRREGULAR TISSUE

Patches were introduced in the homogeneous CV hexagonal model with a reduced connectivity in order to mimic structurally different tissue to the rest of the lattice, such as scar tissue or fibrosis. Luke and Saffitz [41] have shown that fibrosis causes primarily transverse (side-side) decoupling, however longitudinal decoupling (end-end) does also occur.

Two different types of patches were used. Patches of lower local transverse connectivity, ν_{local} demonstrated structural inhomogeneities to the rest of the lattice and can be related to fibrosis which is age related. The second model started with the same global ν as the rest of the lattice and had couples removed to represent the damaging of cells and its resultant decoupling.

These two models differ by the coupling nature within the patch itself. With the local transverse coupling model, transverse connectivity within the patch was reduced while all horizontal couples remained intact. In the percolation model, the lattice was set up as normal. Within the patch, longitudinal or transverse couples were then removed at random. The wavefront within this patch therefore became very disorganised and elongated for this reason. It should be noted that there was still some horizontal bias in this model due to the way the couples were initialised originally.

The patches were constructed by growing them direct from a starter cell. This cell was chosen to be in the very centre of the lattice for ease of visualisation, but could be chosen anywhere. The parameters inputted before growing the patch were the iteration time and the growth probability. In each iteration, newly connected cells to the patch gave each of their neighbours a probability (the growth probability) of joining - starting with the starter cell. The growth probability was later chosen to equal 1 for simplicity and the iteration time was varied across simulations. All cells contained within the patch were stored in a vector that could be referenced to.

Heatmaps based on the number of couples each cell had were produced in order to visualise the location and size of the patch. An example of the heat gradient was shown in figure 13b, where blue was given to a cell with the least number of connections and red represented the most.

LOWER LOCAL TRANSVERSE CONNECTIVITY

After growing the patch, the only variation needed in this model was the initialisation of transverse connections. During the scanning of every cell within the lattice, a check was implemented to determine whether the cell existed in the patch or not. If a cell resided in the patch, the transverse coupling probability was set to a low ν_{local} . If a cell did not, the transverse coupling probability was set to the global coupling probability, ν_{global} - fixed for all simulations. Local ν were chosen at values that would normally send the lattice into AF whereas the fixed ν_{global} was chosen strictly to have no risk.

PERCOLATION THRESHOLD MODEL

In the context of this model, the bonds and sites used to describe percolation theory are analogous to the couples that connect cells to each other and the cells themselves. If a group of cells is said to percolate, it essentially means that there are enough interconnecting couples to be able to travel from a cell at one end via only connected cells to the opposite extreme. At the percolation threshold, there are **just enough** couples for this to occur. In this model, the patch was built to have connectivity at the percolation threshold by redefining this meaning slightly. Rather than a single cell at one end needing to connect to a single cell at the other, at least one cell along the left-hand-side perimeter of the patch had to connect to at least 30% of cells along the right-hand-side of the perimeter. This was to allow waves to still propagate throughout the patch, not a single path.

In this model, the lattice was initialised as normal with the same ν inside and out of the patch. Couples were then removed at random with no longitudinal or transversal bias at a probability of 5% in each iteration. After each iteration, a function was written to check whether the patch still percolated. The function sent a virtual wavefront through the patch, first exciting every cell along the left-hand-side perimeter. If the wavefront activated 30% or more cells along the right hand border, the patch was said to percolate. Couples were then removed at random with the probability of 5% again and the patch was checked to see if it percolated. These steps were repeated until the wavefront could no longer activate 30% of cells on the right-hand border. At this point, couples that were just removed were replaced and the time loop began as normal.

6 RESULTS AND DISCUSSION

6.1 ERRORS

All errors for the following data were quantified using the unbiased maximum likelihood estimate for the standard deviation, $\hat{\sigma}$ [42].

$$\hat{\sigma}^2 = \frac{1}{N-1} \sum_{i=1}^N (\hat{x}_i - \mu)^2 \quad (6.1)$$

Where \hat{x}_i represents individual data values, μ represents the mean across the numerical data range, N represents the number of measurements taken for each data point. The uncertainty on the mean, Σ_μ can then be quantified.

$$\Sigma_\mu = \frac{\hat{\sigma}}{\sqrt{N}} \quad (6.2)$$

6.2 HEXAGONAL AND SQUARE LATTICE

6.2.1 VISUALISATION

Figure 14 shows a homogeneous CV hexagonal lattice as it progresses over time.

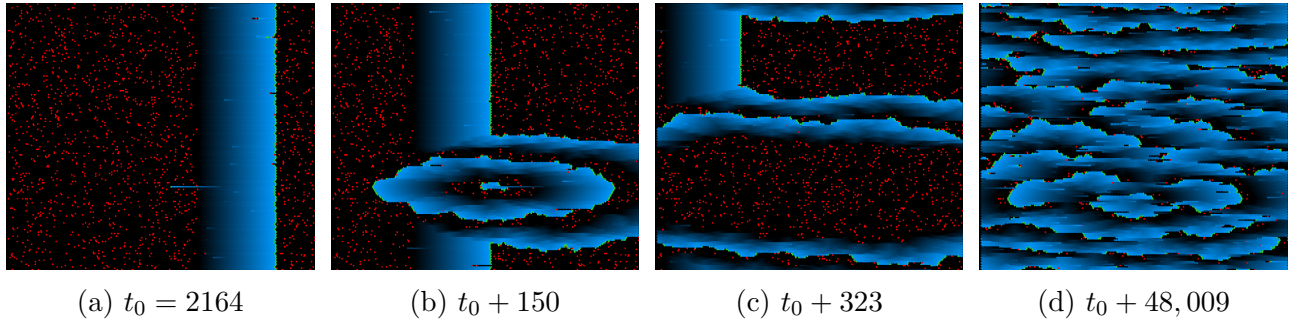


Figure 14: Homogeneous CV on a hexagonal lattice with $\nu = 0.07$ as it progresses over time. The colour scheme is as described in section 5.1. (a) On the verge of reentry, a wavefront can be seen propagating back towards a defective cell that failed to fire. (b) a single rotor forming and self-terminating at a later time (c), analogous to paroxysmal fibrillation. (d) at a much later time, heart rhythm is extremely chaotic and AF will find difficulty in self-terminating, analogous to persistent AF.

A shift is observed. Starting from reentry occurring when a defective cell fails to fire leading to paroxysmal and then further persistent AF. This transition is representative of the shift from transient to recurrent states.

6.2.2 RISK OF FIBRILLATION

The risk of fibrillation, P_{risk} for a homogeneous CV hexagonal and square lattice model is shown in figure 15.

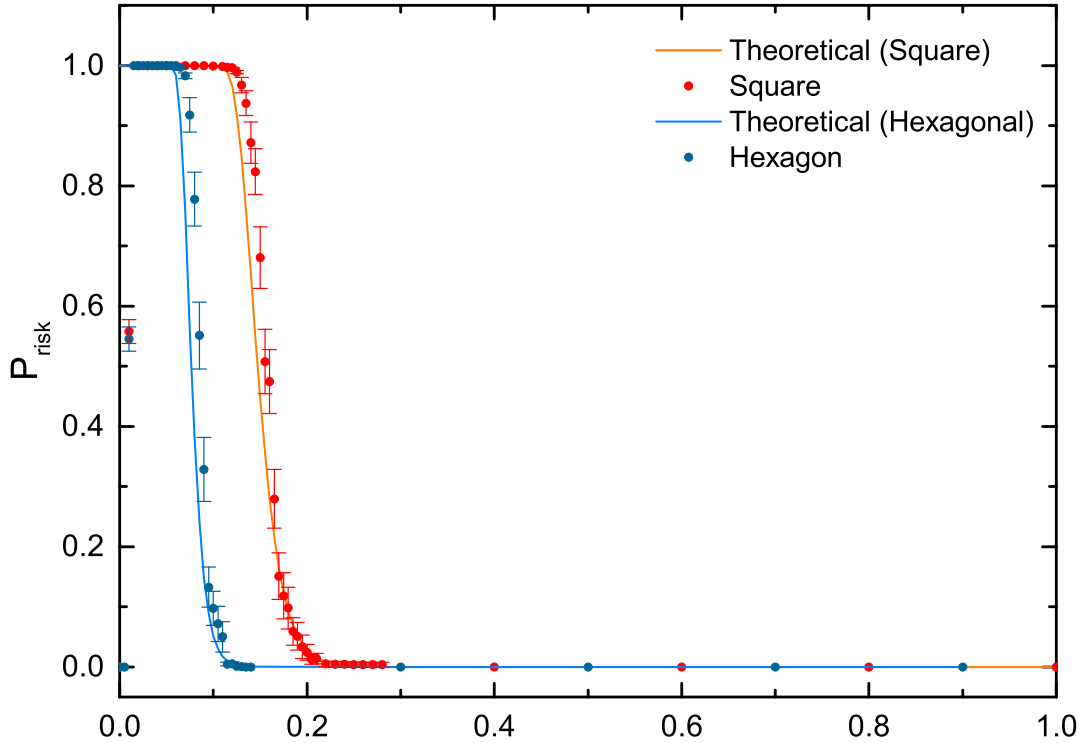


Figure 15: *Numerical Data for Hexagonal and Square Lattice.* The solid lines represent the theoretical fit of P_{risk} for a hexagonal and square lattice (equations 4.4 and 4.5).

A shift to the left for the hexagonal model is observed, and so is less likely to be in a fibrillatory state for a given ν versus the square model. This can be described qualitatively by considering the number of transverse connections. A cell within a hexagonal lattice - with four possible transverse connections - has double the probability of having at least one versus a square cell - which has a possible of two transverse connections. A critical region, as described previously, is dependent upon the distance between a defective cell and its first transverse couple. For a given ν , a cell to the right of a defective cell is more likely to have at least one transverse connection in the hexagonal model and so this distance will generally be shorter, decreasing the likelihood of regions being critical.

For both figures, there is a sharp phase transition that occurs at a critical transverse coupling probability, ν^* . In the hexagonal model, for $\nu \lesssim 0.07$, the system is extremely likely to be in fibrillation and a sharp phase transition is seen past this point. Therefore $\nu^* \approx 0.07$ for a hexagonal lattice. For the square model, this is observed at $\nu^* \approx 0.14$.

6.3 HETEROGENEOUS CONDUCTION VELOCITY

The heterogeneous CV hexagonal model as it progresses over time is shown in figure 16.

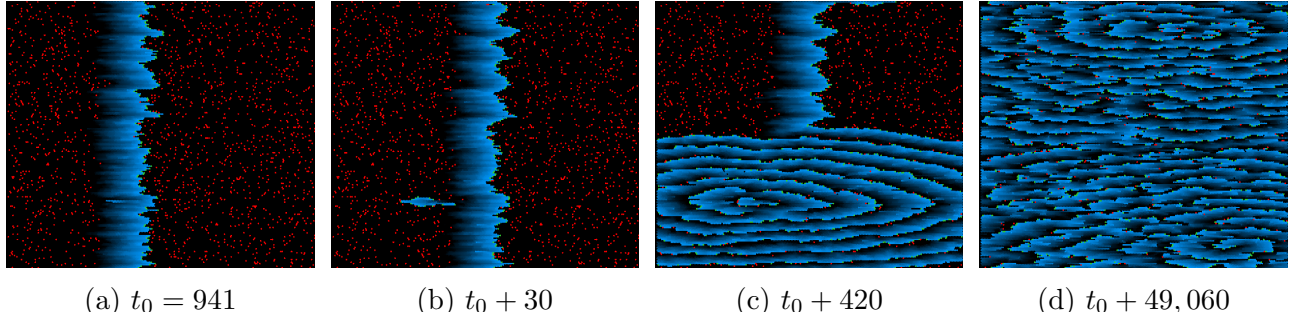


Figure 16: Heterogeneous CV on a hexagonal lattice with $\nu = 0.1$ as it progresses over time. (b) A rotor is initiated. (c) The rotor is visibly increasing in size as wavefronts initiated by it spread through the lattice. (d) The lattice has descended into complete chaos and more rotors are now visible.

Observing the wavefront initiated by the SAN in the first image, there is a clear difference from the homogeneous CV model. The wavefront is jagged as it passes through various cells with differing timedelays. The distance between wavefronts formed by the rotor are also visibly smaller than observed previously. In this example, the system enters AF almost immediately and cannot self-terminate. At a much later time, multiple rotors have formed and the system has descended into complete chaos. This is displaying persistent or possibly even permanent AF.

A histogram for the percentage of cells with a specific timedelay for various values of ν across 50 lattice simulations are displayed in figure 17a.

This can be quantified using a simple binomial probability for a given timedelay.

$$P(\Delta t_c) = \binom{4}{c} \nu^c (1 - \nu)^{4-c} \quad (6.3)$$

Where c is the number of transverse connections, Δt_c represents the value of the timedelay for a given number of transverse connections. This probability is shown schematically in figure 17b.

Numerical data for P_{risk} with heterogeneous CV is shown in figure 18 against previous data found for a hexagonal lattice with homogeneous CV.

A shift to the right is observed versus the homogeneous CV model, this is due to the reduction in CV caused by an increase in timedelay (recall equation 5.1). This reduction in CV causes a reduction in the wavelength, since $\lambda = CV \times \tau$, which means that smaller regions now may be found to be critical. Considering two lattices set up with an identical coupling structure, one with homogeneous CV and one with heterogeneous CV. There will be critical regions found in the heterogeneous model which previously were not, due to a reduction in its wavelength.

Now, a region near a defective cell within this model is considered to be critical when the sum of the timedelays within the reentry circuit are greater than or equal to τ , to allow for cells to the left of the defective cell to leave the refractory stage. Previously this was simply 50 cells.

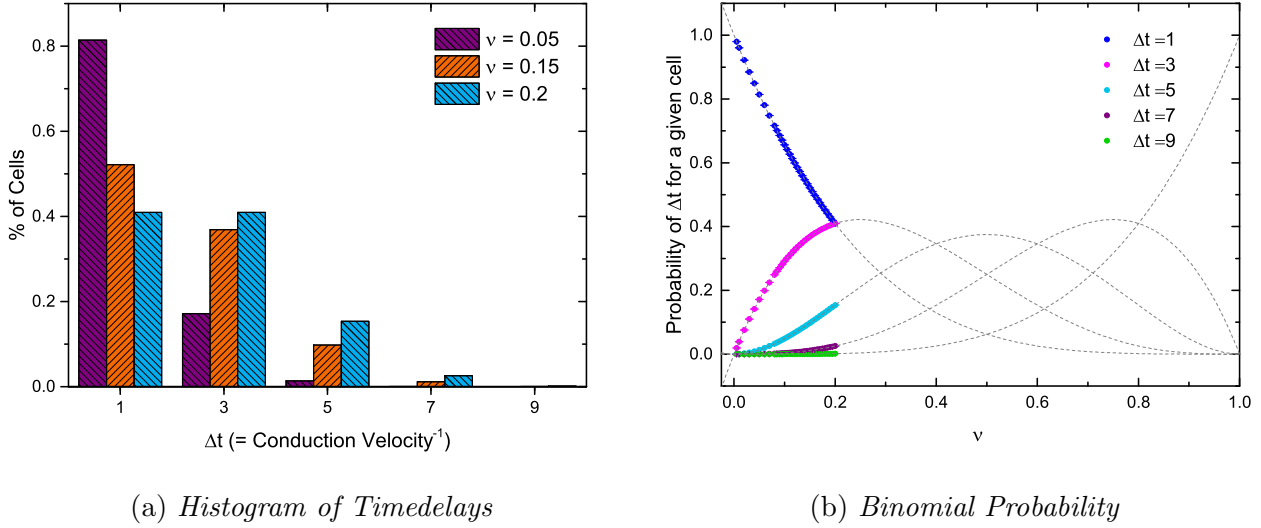


Figure 17: (a) The percentage of cells with a given timedelay for various ν , taken directly from numerical simulations. The percentage of cells with a timedelay of 1 reduces as ν increases. This is anticipated since this represents the percentage of cells with no transverse links. (b) The expected probability for the percentage of cells with a given Δt . The points show numerical results, with the binomial probability plotted over.

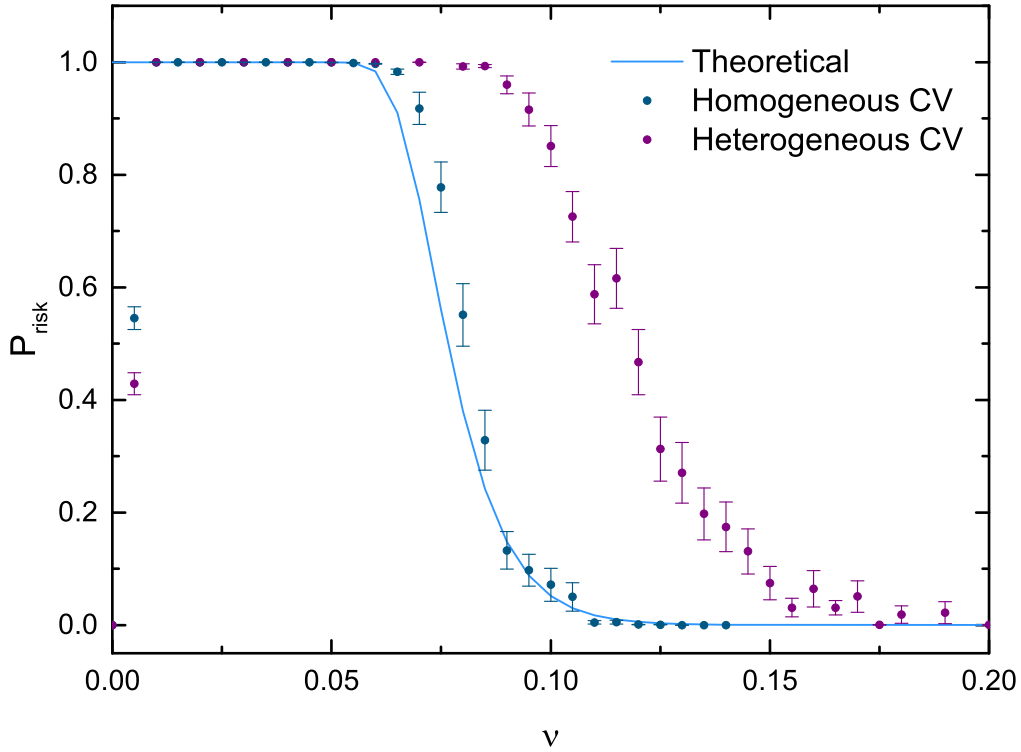


Figure 18: Numerical Data for Heterogeneous CV. The blue data show numerical results for homogeneous CV with the corresponding theoretical curve.

The wavelength is now quantified by the following equation:

$$\sum_{i=0}^{\lambda} \Delta t_i = \tau \quad (6.4)$$

In the heterogeneous CV model, the largest wavelength has been reduced and cannot reach 50 cells. This is because there must be at least two cells within a critical region with at least one transverse connection. The lowest timedelay for a cell with any transverse couples is 3. Therefore making the largest possible reentrant circuit to be 46 cells.

In finding a theoretical fit for this data, a more general form of P_{risk} was reverted to - since the wavelength was no longer simply $\tau = 50$.

$$P_{\text{risk,hex}} = 1 - [1 - (1 - \nu)^{2\lambda}]^{\delta L^2} \quad (6.5)$$

The next task was finding this wavelength, λ for heterogeneous CV. The following sections go through various methods implemented in finding a theoretical fit for P_{risk} using the wavelength. This was necessary in order to understand fully the physical effects of heterogeneous CV on critical regions within the lattice.

6.3.1 AVERAGE TIMEDELAY

The first process calculated an expected average timedelay, $\langle \Delta t \rangle$ for a given ν . The expected wavelength follows from equation (6.4),

$$\langle \lambda \rangle = \frac{\tau}{\langle \Delta t \rangle} \quad (6.6)$$

The expected average time delay for a lattice with a given ν can be calculated using the binomial distribution.

$$\langle \Delta t \rangle = \sum_{c=0}^4 \Delta t_c \binom{4}{c} \nu^c (1 - \nu)^{4-c} \quad (6.7)$$

These values were used to find the expected wavelength and were then inputted into the $P_{\text{risk,hex}}$ equation (6.5) giving the plot shown in figure 19.

It is clear from this graph that the wavelength has been underestimated since there is a shift to the right in comparison with numerical data¹. This naïve assumption assumes no dependency between a critical defective cell and the local coupling of that region. It assumes that all local regions within a given lattice are self-similar and so critical regions could appear anywhere. In reality, critical regions will tend to appear in areas of lower local transverse connectivity in comparison to the outside tissue because the distance from a defective cell to its first vertical couple will be increased thus improving the likelihood these regions are indeed critical. If the local coupling of a critical region is overestimated, the wavelength will become an underestimate (see equation 6.6).

¹ Positions to the right of the numerical results means that there is an underestimate of the wavelength, positions to the left mean there is an overestimate of the wavelength.

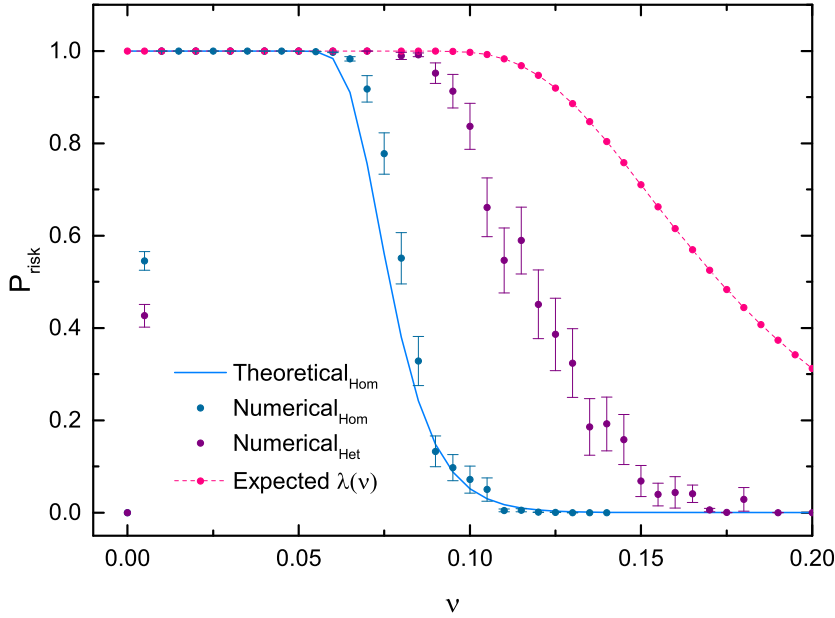


Figure 19: *Expected Wavelength*. The expected wavelength (shown in pink) versus numerical data (purple) with homogeneous CV data for comparison.

6.3.2 EXTREMAL STATISTICS

Methods employed in the previous section did not offer comparable results to numerical data and so the next approach aimed at using extremal statistics to find a better theoretical fit.

In finding the wavelength for a specific ν , maximal values were taken due to the previous underestimation of the wavelength. Lattices using 300 seeds were simulated for every given value of ν . The number of critical regions, N present in each lattice were then counted and averaged across all seeds.

This time, the wavelength was described via a **random** selection of cells whose time delays sum to τ - see equation 6.4. A wavelength was recorded N times and extremal values were taken.

The process in finding an extremal value for the wavelength was as follows. Scanning through every value of ν :

1. Initialise lattice for given ν and seed.
2. Randomly select a cell from the lattice, sum timedelay and remove.
3. Repeat step 2 until equation 6.4 is satisfied.
4. Record the number of cells needed to satisfy equation 6.4, the wavelength.
5. Repeat steps 2 through 4, N times (the number of critical regions present for a given ν).
6. Take maximal value of recorded wavelengths.

These maximal values found for the wavelength, $\lambda_{\max}(\nu)$ were then averaged across all seeds and input into $P_{\text{risk},\text{hex}}$, equation 6.5. The result is shown in figure 20 with the expected wavelength for comparison.

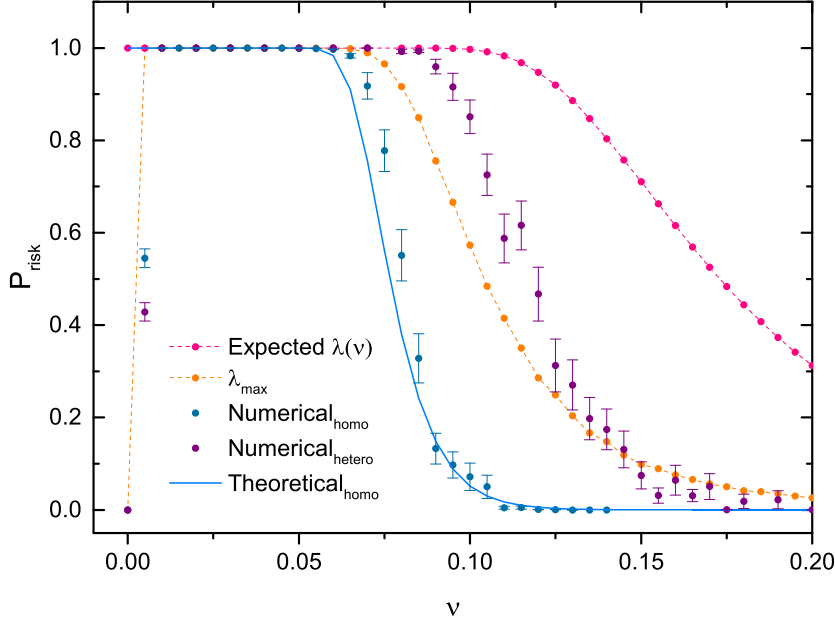


Figure 20: *Maximal Wavelength Values.* Maximal data taken for the wavelength for each individual ν (orange) versus the previous expected wavelength (pink).

Maximal values fit better for reasons previously described in section 6.3.1. Critical regions will tend to appear in regions of lower local connectivity thus areas where the wavelength is larger. This seems slightly contradictory when considering that a reduction in the wavelength can result in smaller critical regions. Although this fits for the shift between the homogeneous CV and heterogeneous CV model, the same cannot necessarily be said for P_{risk} within the heterogeneous CV model across all ν . The wavelength, by definition is derived from connectivity. The connectivity of a local region is the ultimate factor in deciding whether it is critical, although a smaller wavelength can help. Although counter-intuitive, a larger wavelength is more likely to facilitate a rotor since there must be fewer transverse connections within this region.

Although taking a maximum wavelength has shown far more comparable to numerical data, it clearly is not showing the full picture since the gradient is too shallow. This fit was found by taking a random selection of cells, it ignores the actual structure of the cell-cell coupling and only takes into account their timedelays. The structural coupling of cells is of huge importance in determining whether a rotor can form or not. This effect is most noticeable for extremal ν . For very low values, there is a balance between finding a group of cells of maximal wavelength and those cells actually able to facilitate a rotor. The most obvious example of this is where the simulation found that $\lambda_{\max} > 46$. A rotor cannot physically form for values greater than this in the heterogeneous model.

This figure highlights the overestimation of the wavelength for values $\nu \lesssim 0.145$. For critical values of ν (where the sharp decrease in P_{risk} is observed), there seems a fine balance between the importance of local areas with the lowest connectivity versus slightly larger connectivity and therefore a smaller wavelength. With lowest connectivity, the wavelength is maximal. For slightly larger connectivity, the physical coupling structure necessary to facilitate a rotor is rarer. The figure suggests that for critical values, these rarer, smaller wavelengths are of greater importance, hence an overestimation using λ_{\max} .

6.3.3 WEIGHTED TIMEDELAY

The final method aimed to find a global wavelength across all ν . Weighted values of the timedelay based on their corresponding value in P_{risk} were used in determining this global wavelength.

Looking at figure 21, the number of critical regions dramatically decreases for larger ν . Regardless of any wavelength chosen for large ν , a critical region of any size can never form because there are simply too many transverse connections. It was determined that higher values of ν have less influence over the global wavelength since these systems can never facilitate a rotor. The weighting against values of P_{risk} were used as a means of measuring the importance of a particular ν in determining the wavelength. Higher values therefore had less weighting on the global wavelength, since the number of critical regions within these lattices were far smaller if not zero.

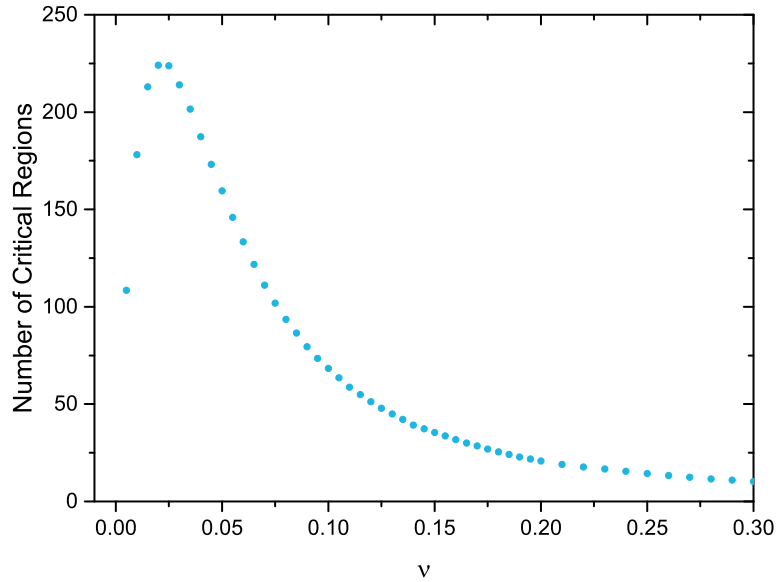


Figure 21: *Number of Critical Regions for Heterogeneous CV for a Given ν .* The sharp decrease tends to zero as ν increases. A system can only enter AF if there is at least one critical region.

The weighted average timedelay, $\overline{\Delta t}$ was determined by the following equation.

$$\overline{\Delta t} = \frac{\sum_{\nu=0}^1 \langle \Delta t_\nu \rangle P_{\text{risk}}(\nu)}{\sum_{\nu=0}^1 P_{\text{risk}}(\nu)} \quad (6.8)$$

This was first calculated using numerical results found for P_{risk} . This can then be inputted back into the P_{risk} equation with the new wavelength.

$$P_{\text{risk}} = 1 - \left[1 - (1 - \nu)^{\frac{2\tau}{\overline{\Delta t}}} \right]^{\delta L^2} \quad (6.9)$$

6. Results and Discussion

Following through with the same process, now using the theoretical P_{risk} just found opposed to numerical results, the following steps were iterated through a number of times.

1. Find $\bar{\Delta t}$ using equation for P_{risk} , (6.9)
2. Using new found $\bar{\Delta t}$, input back into (6.9)
3. Return to step 1

The wavelength found using this weighted average converged to a single value. This process is demonstrated in figure 22.

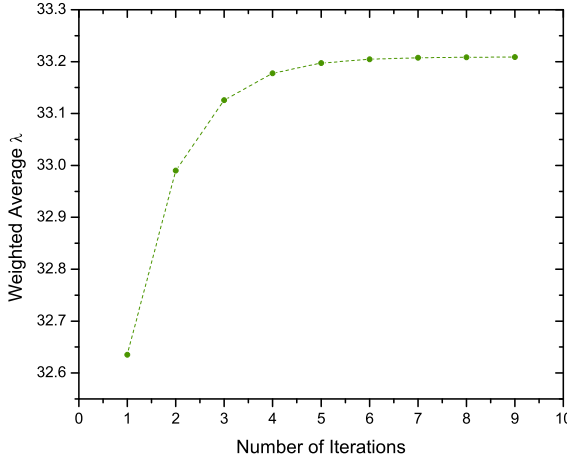


Figure 22: Value for the Weighted Wavelength Over a Number of Iterations.

The iteration gave a final wavelength of $\bar{\lambda} = 33.21$. The P_{risk} fit produced is shown in figure 23. The gradient now visibly fits numerical data far better than previously found, suggesting a global wavelength across all ν presents a truer picture.

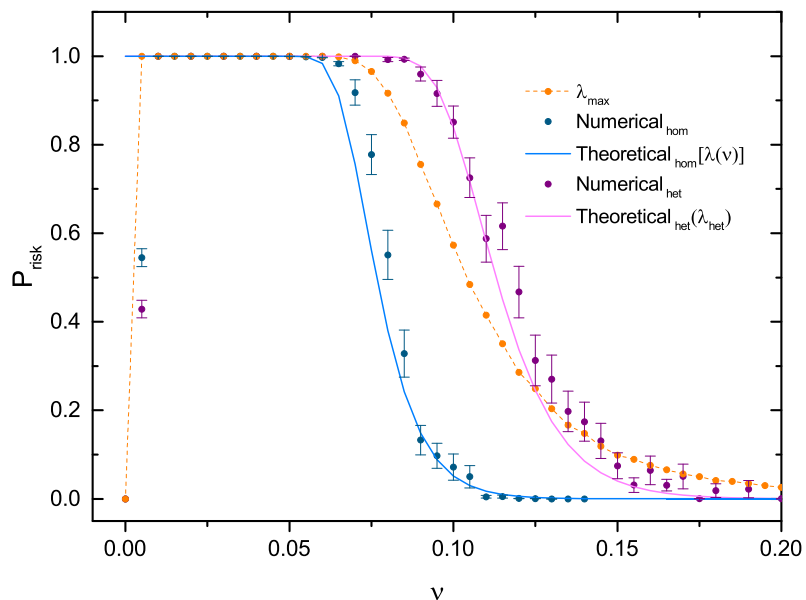


Figure 23: Weighted Average Wavelength. P_{risk} using a weighted wavelength (purple solid line) versus the previous maximal wavelength chosen for individual ν (orange).

6.4 RISK OF FIBRILLATION FOR ALL MODELS

The final graph for all P_{risk} curves along with the chosen theoretical fit for the heterogeneous CV model is shown in figure 24. The weighted timedelay fit was chosen for the heterogeneous CV hexagonal model since the gradient fitted better than any other wavelengths tested.

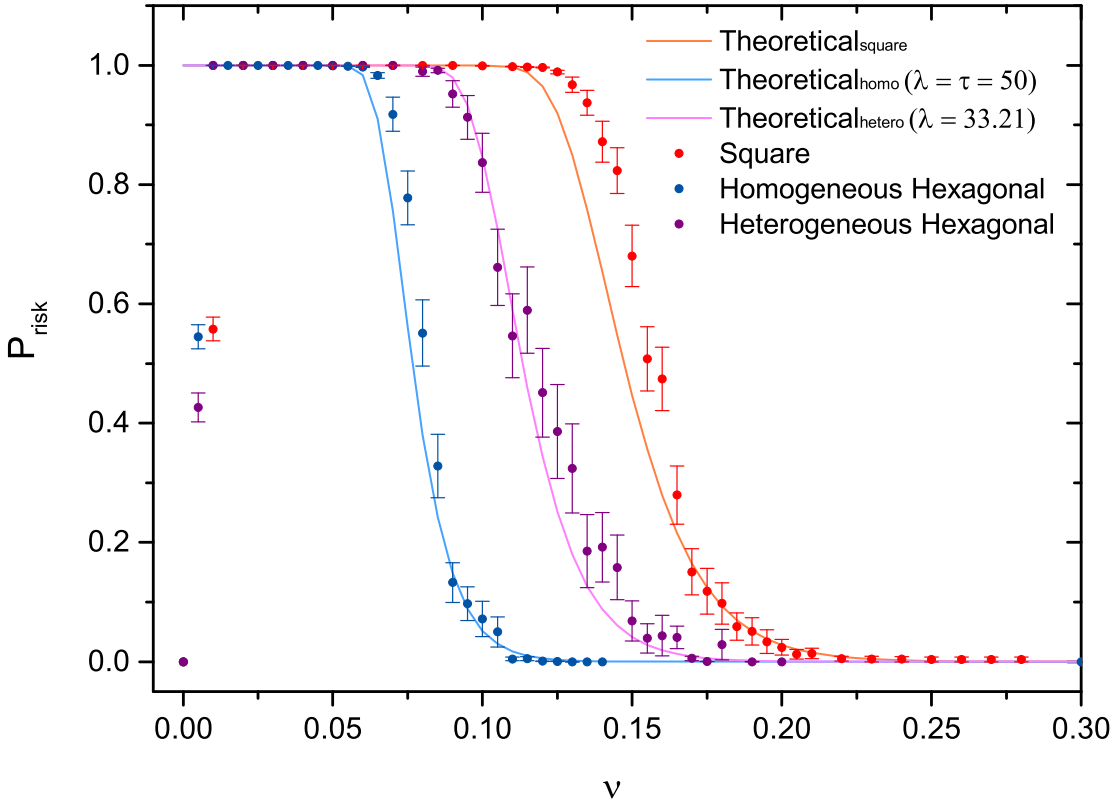


Figure 24: *Final P_{risk} for all Models.* Numerical data for all models with theoretical fits plotted as solid lines. The chosen theoretical fit for the heterogeneous CV hexagonal model (purple) used a global wavelength across all ν , $\lambda = 33.21$. Theoretical fits for the homogeneous CV models the equation for the probability of at least one critical defective cell existing in a lattice.

6.5 PATCHES OF IRREGULAR TISSUE

The critical distance between a defective cell and its first vertical couple in the homogeneous CV model is equal to half the wavelength, in this case $\tau/2$. This can be extended to a critical size of patch needed to induce AF. The critical radius, R_{crit} of a patch is half this critical distance,

$$R_{\text{crit}} = \frac{\tau}{4} = 10.25 \quad (6.10)$$

It is expected that this is the minimum radius of patch needed to induce AF, and AF cannot occur for a radius of patch smaller than this value.

6.5.1 REDUCED LOCAL TRANSVERSE COUPLING PROBABILITY

The progression over time for a patch of radius 40 at a local coupling probability, $\nu_{\text{local}} = 0.05$ and global coupling of $\nu_{\text{global}} = 0.2$ is shown in figure 25. A heatmap showing the connectivity has been superimposed in order to visualise the location of reentry with regards to the patch. The colour scheme for refractory and excited states has been changed for ease of visualisation over the heatmap. Refractory states are now shown in pink with excited cells in white.

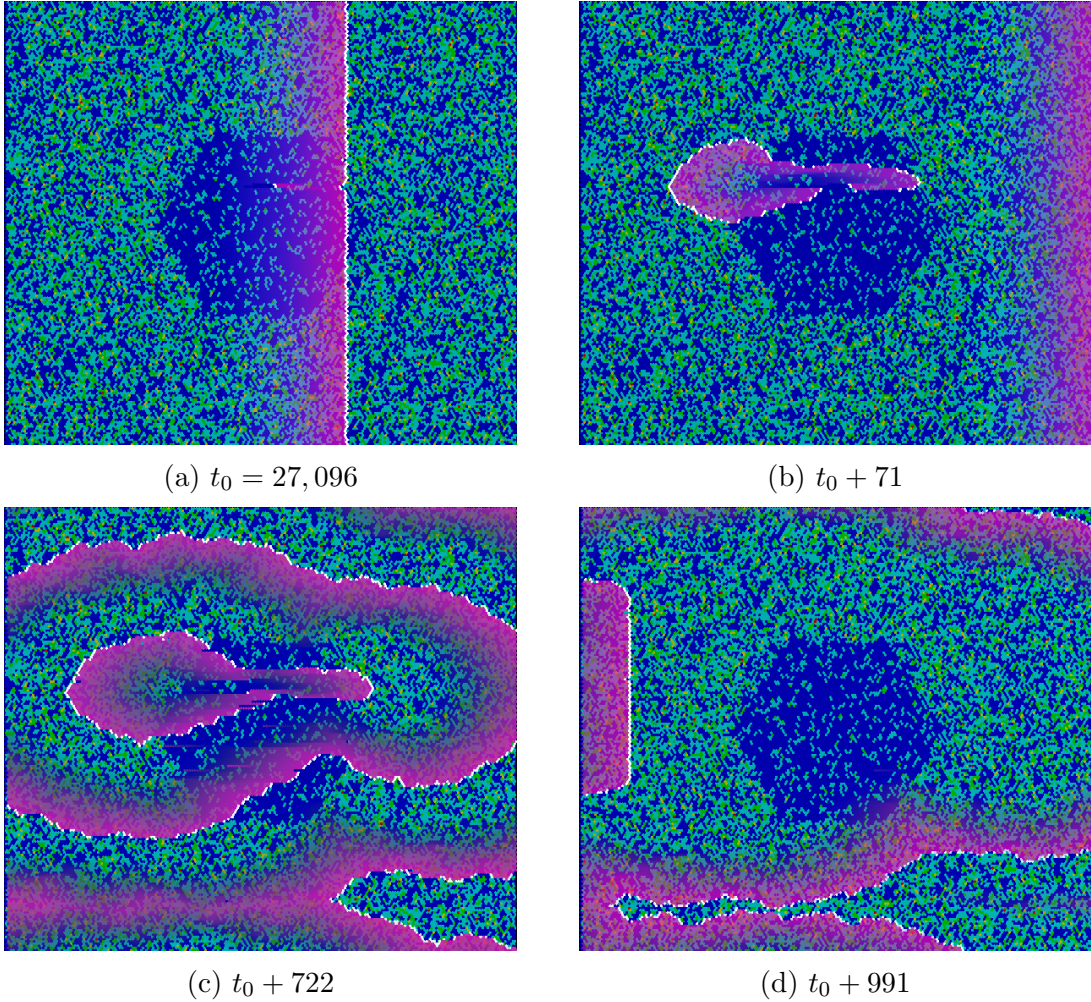


Figure 25: *Progression Over Time for a Patch of Radius 40 with $\nu_{\text{local}} = 0.05$.* A lattice set up with $\nu = 0.05$ usually has a probability of entering AF equal to 1. The outside tissue, with $\nu = 0.2$ would usually have zero probability of entering AF. Paroxysmal AF is observed, initiated in the patch but terminating at a later time (d).

The patch forces the system into paroxysmal AF. The local coupling probability would usually give a P_{risk} of 1. However, the radius clearly is not large enough to send the system into complete chaos and it can still self-regulate at intervals.

The kinked wavefront observed as it leaves the patch is due to the path of the wave as reentry is occurring. The reentrant wave travels close towards the left side of the patch before turning back on itself. When the left part of the wave leaves the patch, it encounters more transverse connections and therefore spreads outwards. The reentrant wave travelling back on itself only encounters many transverse connections as it leaves the patch on the right-hand-side, at which point it spreads outwards. The left part of this wavefront therefore has been given more time to advance in the transverse direction hence we see the kinked nature.

Results of P_{risk} for varying radii and ν_{local} are shown in figure 26. Indeed, we see that for a

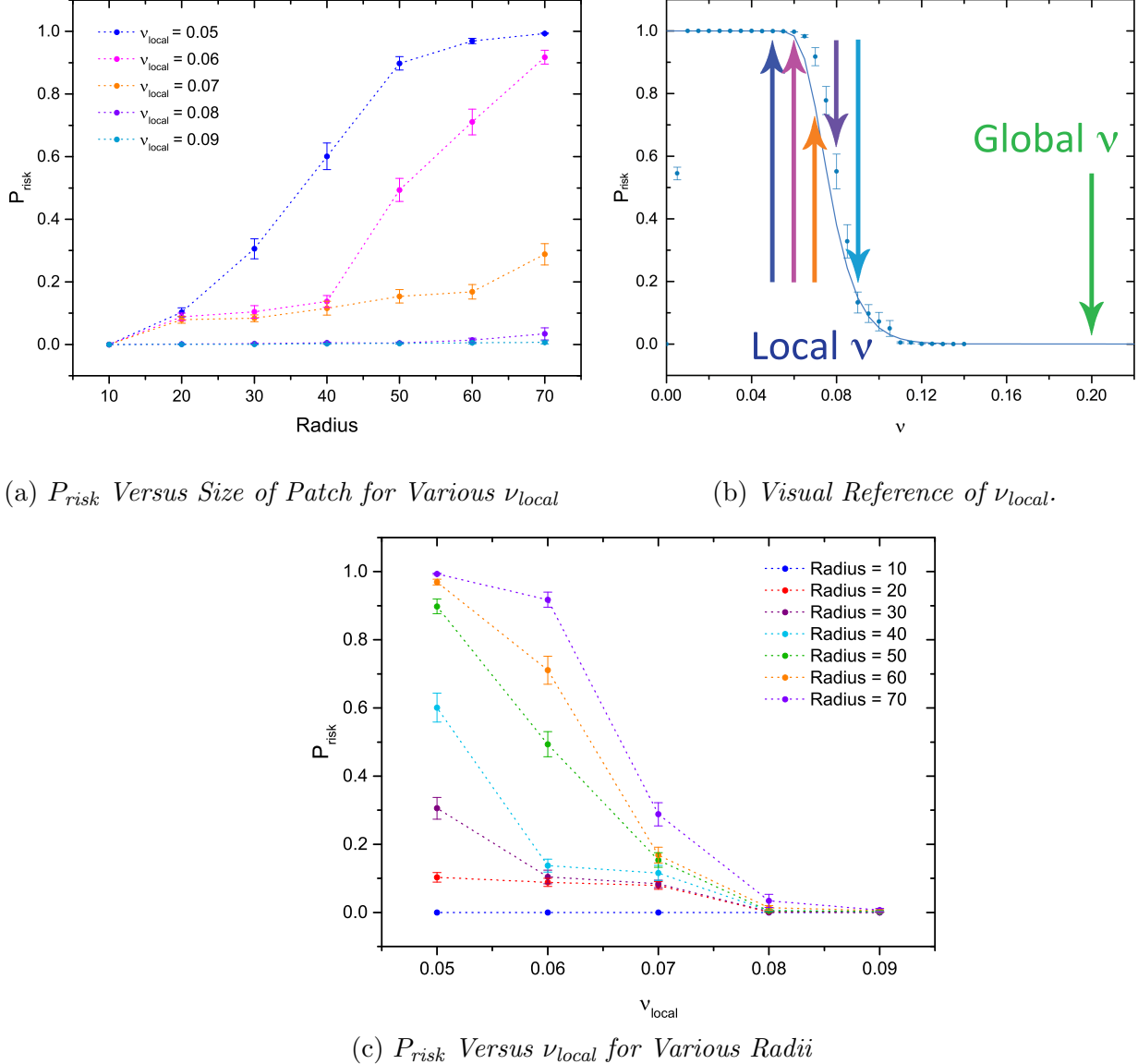


Figure 26: (a) Values obtained for P_{risk} with various radii of the patch and various ν_{local} . (b) Visual reference for ν_{local} and ν_{global} to where they would usually lie on the P_{risk} figure. (c) Identical data to (a) plotted with ν_{local} along x-axis.

radius of 10 for all values of ν_{local} , the system can never enter AF - consistent with the expected critical radius, $R_{\text{crit}} = 10.25$.

The values obtained for P_{risk} also seem highly dependent on where these values of ν_{local} would usually reside on the P_{risk} figure. Values for ν_{local} of 0.08 and 0.09 (with non-zero P_{risk} usually) find it extremely difficult to force the system AF even for a radius of 70. Only ν_{local} giving a P_{risk} of 1 are almost certain to increase P_{risk} dramatically.

6.5.2 CONNECTIVITY AT THE PERCOLATION THRESHOLD

The progression over time for a patch of radius 40 at the percolation threshold with a global coupling of $\nu_{\text{global}} = 0.2$ is shown in figure 25. The colour scheme has been changed for reasons stated in section 6.5.1.

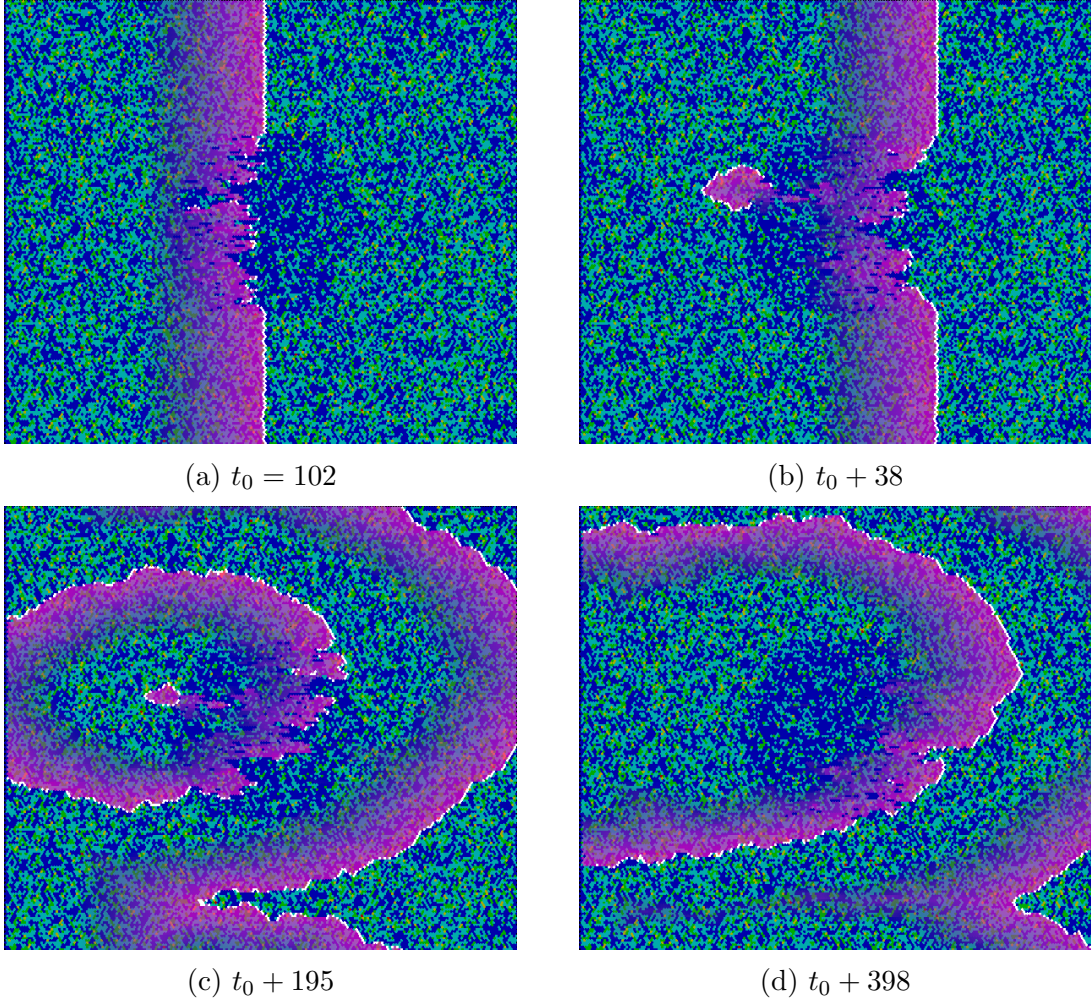


Figure 27: *Progression Over Time for a Patch of Radius 40 at the Percolation Threshold with Outside Tissue at $\nu = 0.2$.* (a) The wavefront is visibly different as it enters the patch as small fronts undergo multiple deflections. (b) A reentrant wavefront is initiated due to these deflections and sends the system into AF. The patch cannot sustain AF and it self-terminates at a later time (d) - representative of paroxysmal AF.

As the wavefront enters the patch, it undergoes winding paths due to the unbiased decoupling of cells. Reentry starts at the border of the patch, entering the outside tissue immediately. Alonso and Bär [43] conducted an experiment introducing areas of tissue with non-conducting couples set at the percolation threshold in a homogeneous medium and similarly found the wavefront emanating from the border of the patch causing reentry within the outside tissue.

AF is induced by the deflected path the wavefront undergoes as it enters the patch and is not necessarily the result of a defective cell not firing. The zigzag paths from cell to cell send the wavefront back towards the SAN, meeting re-excitable tissue as the wavefront leaves the patch. The way in which AF can be induced has changed, and can be solely due to the structure of connections - a defective cell is no longer necessary.

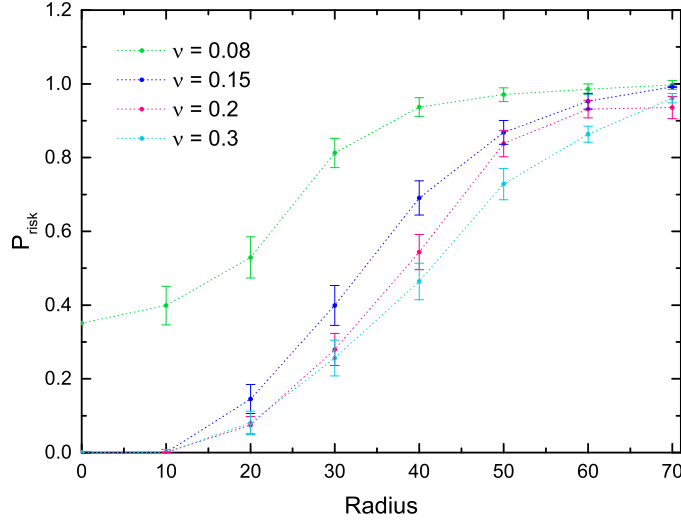


Figure 28: P_{risk} Versus Size of Patch at the Percolation Threshold for Various ν_{global} . A radius of zero is also displayed to show normal values expected for P_{risk} .

Results of P_{risk} for varying radii and ν_{global} are shown in figure 28. Again, AF cannot occur for a radius of 10 as expected.

For values of ν that would usually give a P_{risk} of zero, we see very similar plots. Because the connectivity of the patch is set to the percolation threshold for every ν , it does not differ greatly across simulations. We would expect that if outside tissue perpetuated AF, we would see a decrease in P_{risk} with an increase in ν . This suggests that the patch is the initiator and perpetuator of AF, since there is no real variation within the patch itself.

A $\nu_{\text{global}} = 0.08$ which is a critical value and gives non-zero P_{risk} differs from the other results. This model has a higher risk of entering AF which would be expected. In this system, it is possible for the AF to be initiated within the patch but perpetuated in the outside tissue and so it would be expected that the system finds more difficulty in self-regulating.

6.5.3 COMPARISON OF BOTH MODELS

Figures 25 and 27 with a radius of 40 and a global transverse coupling probability of $\nu_{\text{global}} = 0.2$ display differing characteristics, for example the way in which reentry occurs. For the patch of lower local transverse connectivity, AF is initiated within the patch. In the percolation model, reentry is initiated at the boundary between the patch and the outside tissue. Also, the local transverse connectivity model must have a defective cell driving reentry, whereas the percolation model does not.

Similarities between these two systems include the type of AF that is initiated and the alteration in the wavefront. Both systems display paroxysmal AF. Although the patches induce AF, the system in both cases manages to self-regulate at intervals. The patches also clearly have an affect on the shape of the wavefronts that emerge during reentry. The distance between wavefronts that have emerged from rotors are much larger in comparison to no patch present (see figures 14, 25 and 27). Because this distance is large, it is not surprising the system easily self-regulates as there are still many resting cells able to be excited when the SAN initiates another wavefront.

Figure 29 compares the results of a patch with lower local transverse connectivity and a patch at the percolation threshold for $\nu_{\text{global}} = 0.2$. This value was chosen for a fair comparison since all values of ν_{global} are equal.

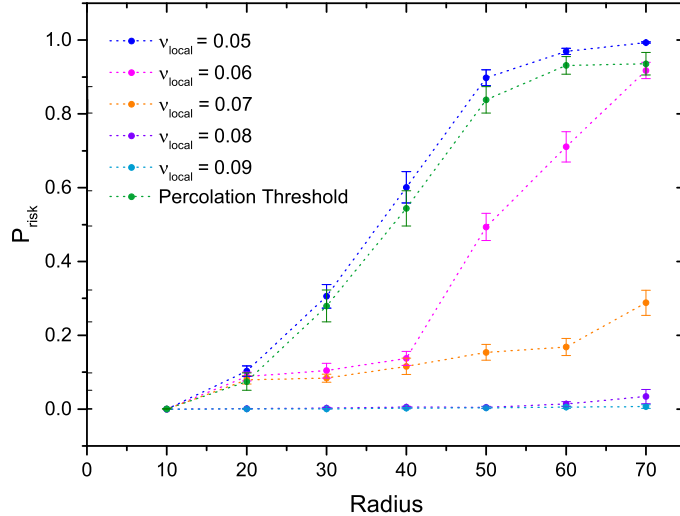


Figure 29: *Comparison of Irregular Tissue.* Data for patches of various ν_{local} are displayed with a patch at the percolation threshold at $\nu_{\text{global}} = 0.2$.

The main thing to note from this figure is the almost identical P_{risk} for $\nu_{\text{local}} = 0.05$. The expected number of couples per cell for $\nu = 0.05$ is 2.20. This is comparable for the average number of couples per cell for the percolation data, which was found to be 2.17. Although these are very similar, the coupling structures within the patch will be hugely different. The way in which AF is induced is also likely to be very different (see figures 25 and 27). However, the system clearly self-regulates in a similar way for both models and both patches cause similar effects (though for different reasons) since we get similar results.

7 CONCLUSIONS AND FUTURE STUDY

Atrial fibrillation is the most common cardiac arrhythmia and a major cause of stroke. Despite this, the mechanics are still not fully understood. A direct link between age and AF, accompanied by an ageing population means the understanding of its mechanics are becoming increasingly important for the aid in its treatment. With better understanding of the complexities the heart undergoes during AF, the form of localised sources may become more easily identifiable potentially benefitting better diagnosis in patients. Computational models are popular for their ability of identifying critical regions and fast simulation results that can be achieved.

This project used a cellular automaton (computational) model, discretising the cardiac muscle cells. The original model built on the work of Christensen and Manani [40], using a square lattice grid to represent the cardiac cells and equivalent results were verified. This model was then extended to replicate further characteristics of the heart cells and model possible critical structures in the form of irregular tissue. The square lattice was replaced with a hexagonal grid to model more closely the coupling structure within the myocardium. Heterogeneous conduction velocity was also introduced based on the coupling of an individual cell. Additionally, patches of structurally different tissue was introduced in order to model the possible initiation of AF via anatomical obstacles.

The heterogeneous CV model, reduced the wavelength of reentry thereby increasing the risk of fibrillation. The simplified model of the source-sink affect on CV generalised this concept to the number of connections a cell has. This could have been studied further, increasing its complexity by considering the number of sources conduction was being received by a particular cell versus the number of cells it was giving conduction to for every timestep.

Patches representing damaged tissue or fibrosis were found to induce AF. However, these were not able to perpetuate it, displaying paroxysmal atrial fibrillation where the system caused the arrest of rotors at regular intervals. The wavefronts emanating from rotors were also found to be visibly different to rotors formed within a patch-free tissue. These could thus be identified as critical structures within the heart and AF was not induced or perpetuated by the general tissue. With more time, this could have been studied further by using heterogeneous CV as well as modelling more patches. Observing the induced effects and whether atrial fibrillation can be perpetuated may lead to further recognition of these structures within real atria.

The extension of the original model has highlighted new aspects that could be deemed important in human studies and to this end, many of the project aims have been met. There is however ample room for further study within these extensions.

8 ACKNOWLEDGEMENTS

Firstly, I would like to thank my project supervisor Professor Kim Christensen whose passion and guidance has helped the work undertaken tremendously. Thank you for providing me and my partner with such a fantastic project, I have truly enjoyed helping with your research this year.

Secondly, to Professor Kim Christensen's PhD student Kishan Manani whose helpful and friendly nature has helped the project go smoothly. Thank you so much for all the advice and guidance you have offered throughout the year and for answering the many questions we have had as well as providing us with useful papers. Your approachable character and clear way of explaining things has helped us substantially when we have been unsure and confused.

Lastly to my project partner, throughout this year you have offered a tremendous amount of support. Without you, this project could not have gone ahead. Your clear mind and enthusiastic nature have been crucial to the success of this project and you have undoubtedly made it more enjoyable.

REFERENCES

- [1] S Nattel. New ideas about atrial fibrillation 50 years on. *Nature*, 415(6868):219–225, 2002.
- [2] M Haïssaguerre, P Jaïs, D. C. Shah, A Takahashi, M Hocini, G Quiniou, S Garrigue, A Le Mouroux, P Le Métayer, and J Clémenty. Spontaneous initiation of atrial fibrillation by ectopic beats originating in the pulmonary veins. *New England Journal of Medicine*, 339(10):659–666, 1998.
- [3] J. L. Cox, R. B. Schuessler, and J. P. Boineau. The development of the maze procedure for the treatment of atrial fibrillation. *Seminars in Thoracic and Cardiovascular Surgery*, 12(1):2–14, 2000.
- [4] R. H. Clayton. Computational models of normal and abnormal action potential propagation in cardiac tissue: linking experimental and clinical cardiology. *Physiological Measurement*, 22(3):R15–R34, 2001.
- [5] R Nave. Heart electrical phenomena. <http://hyperphysics.phy-astr.gsu.edu/hbase/biology/heartelec.html>. Accessed: 12/10/2014.
- [6] A. E. Buxton, K. E. Ellison, M. M. Kirk, and G. F. Michaud. Introduction to cardiac electrophysiology, the electrocardiogram, and cardiac arrhythmias. http://www.brown.edu/Courses/Bio_281-cardio/cardio/EKGhandout1.pdf, 2014.
- [7] J. P. Keener and J Sneyd. *Mathematical Physiology, I, Cellular Physiology*. Springer, 2nd edition, 2008.
- [8] <http://musom.marshall.edu/graphicdesign/ibooks/website-portfolio-images/Systems/Cardiovascular%20Normal/Cardiac%20Action%20Potential-MU.jpg>. Accessed: 12/10/2014.
- [9] M. S. Spach and P. C. Dolber. Relating extracellular potentials and their derivatives to anisotropic propagation at a microscopic level in human cardiac muscle: Evidence for electrical uncoupling of side-to-side fiber connections with increasing age. *Circulation Research*, 58:356–371, 1986.
- [10] Myocardium. <http://www.humpath.com/spip.php?article3277>, 2004.
- [11] J. E. Saffitz, H. L. Kanter, K. G. Green, T. K. Tolley, and E. C. Beyer. Tissue-specific determinants of anisotropic conduction velocity in canine atrial and ventricular myocardium. *Circulation Research*, 74:1065–1070, 1994.
- [12] T Koura et al. Anisotropic conduction properties in canine atria analyzed by high-resolution optical mapping: Preferential direction of conduction block changes from longitudinal to transverse with increasing age. *Circulation*, 105:2092–2098, 2002.
- [13] P Spector. Principles of cardiac electric propagation and their implications for re-entrant arrhythmias. *Circulation: Arrhythmia and Electrophysiology*, 6:655–661, 2013.
- [14] R. B. Schuessler, T. M. Grayson, B. I. Bromberg, J. L. Cox, and J. P. Boineau. Cholinergically mediated tachyarrhythmias induced by a single extrastimulus in the isolated canine right atrium. *Circulation Research*, 71(5):1254–1267, 1992.
- [15] J Jalife, O Berenfeld, and M Mansour. Mother rotors and fibrillatory conduction: a mechanism of atrial fibrillation. *Cardiovascular Research*, 54(2):204–216, 2002.

REFERENCES

- [16] How atrial fibrillation progresses. <http://www.stopafib.org/progresses.cfm>. Accessed 16/04/2015.
- [17] W. E. Garrey. Auricular fibrillation. *Physiological Reviews*, 4(2):215–250, 1924.
- [18] A Rosenblueth and J Garcia Ramos. Studies on flutter and fibrillation: II. the influence of artificial obstacles on experimental auricular flutter. *American Heart Journal*, 33(5):677–684, 1947.
- [19] H Winterberg. Studien über herzflimmern. I. über die wirkung des n. vagus und accelerans auf das flimmern des herzens. *Pflugers Arch Ges Physiol*, 117:223–256, 1907.
- [20] D Scherf, F. J. Romano, and R Terranova. Experimental studies on auricular flutter and auricular fibrillation. *American Heart Journal*, 36(2):241–251, 1948.
- [21] G. R. Mines. On dynamic equilibrium in the heart. *J Physiol (London)*, 46:349–383, 1913.
- [22] G. K. Moe and J. A. Abildskov. Atrial fibrillation as a self-sustaining arrhythmia independent of focal discharge. *American Heart Journal*, 58(1):241–255, 1959.
- [23] M. A. Allessie, W. J. E. P. Lammers, F. I. M. Bonke, and J Hoellen. Experimental evaluation of moe's multiple wavelet hypothesis of atrial fibrillation. In *Cardiac Electrophysiology and Arrhythmias*, pages 265–276, 1985.
- [24] M. A. Allessie, F. I. M. Bonke, and F. J. G. Schopman. Circus movement in rabbit atrial muscle as a mechanism of tachycardia. III. the "leading circle" concept: A new model of circus movement in cardiac tissue without the involvement of an anatomical obstacle. *Circulation Research Journal of the American Heart Association*, 41(1):9–18, 1977.
- [25] A Grace. Atrial fibrillation: Focal sources, rotors and spirals. <http://www.heartrhythmcongress.com/files/file/HRC2012%20Presentations/120925-1145-Focal%20sources,%20rotors%20and%20spirals,%20A%20Grace.pdf>, 2012. Accessed 05/10/2014.
- [26] G. K. Moe, W. C. Rheinboldt, and J. A. Abildskov. A computer model of atrial fibrillation. *American Heart Journal*, 67(2):200–220, 1964.
- [27] J Jalife. Rotors and spiral waves in atrial fibrillation. *Journal of Cardiovascular Electrophysiology*, 14(7):776–780, 2003.
- [28] A. C. Skanes, R Mandapati, O Berenfeld, J. M. Davidenko, and J Jalife. Spatiotemporal periodicity during atrial fibrillation in the isolated sheep heart. *Circulation*, 98(12):1236–1248, 1998.
- [29] R Mandapati, A Skanes, J Chen, O Berenfeld, and J Jalife. Stable microreentrant sources as a mechanism of atrial fibrillation in the isolated sheep heart. *Circulation*, 101(2):194–199, 2000.
- [30] M Mansour, R Mandapati, O. J. Berenfeld, J Chen, F. H. Samie, and J Jalife. Left-to-right gradient of atrial frequencies during acute atrial fibrillation in the isolated sheep heart. *Circulation*, 103(21):2631–2636, 2001.
- [31] Morillo C. A., G. J. Klein, D. L. Jones, and C. M. Guiraudon. Chronic rapid atrial pacing. structural, functional, and ep characteristics of a new model of sustained atrial fibrillation. *Circulation*, 91(5):1588–1595, 1995.

- [32] M Reumann, J Bohnert, B Osswald, S Hagl, and O Doessel. Multiple wavelets, rotors, and snakes in atrial fibrillation a computer simulation study. *Journal of Electrocardiology*, 40(4):328–334, 2007.
- [33] M Gerhardt, H Schuster, and J. J. Tyson. A cellular automaton model of excitable media including curvature and dispersion. *Science*, 247(4950):1563–1566, 1990.
- [34] P Ruchat, N Virag, L Dang, J Schlaepfer, E Pruvot, and L Kappenberger. A biophysical model of atrial fibrillation ablation: what can a surgeon learn from a computer model? *Eurospace*, 9:vi71–vi76, 2007.
- [35] B Chopard and M Droz. *Cellular Automata Modeling of Physical Systems*. Cambridge University Press, 1998.
- [36] N Wiener and A Rosenblueth. The mathematical formulation of the problem of conduction of impulses in a network of connected excitable elements, specifically in cardiac muscle. *Archivos de cardiología de México*, 16(3):205–265, 1946.
- [37] J. M. Greenberg and S. P. Hastings. Spatial patterns for discrete models of diffusion in excitable media. *SIAM*, 34(3):515–523, 1978.
- [38] G Bub, A Shrier, and L Glass. Spiral wave generation in heterogeneous excitable media. *Physical Review Letters*, 88(5):058101, 2002.
- [39] G Bub, A Shrier, and L Glass. Global organization of dynamics in oscillatory heterogeneous excitable media. *Physical Review Letters*, 94(2):028105, 2005.
- [40] K Christensen, K. A. Manani, and S. P. Nicholas. A simple model for identifying critical structures in atrial fibrillation. *Physical Review Letters*, 114:028104, 2015.
- [41] R. A. Luke and J. E. Saffitz. Remodeling of ventricular conduction pathways in healed canine infarct border zones. *Journal of Clinical Investigation*, 87:1594–1602, 1991.
- [42] R Trotta. Statistics of measurement: Summary handout, 2012.
- [43] S Alonso and M Bär. Reentry near the percolation threshold in a heterogeneous discrete model for cardiac tissue. *Physical Review Letters*, 110:158101, 2013.
- [44] E. W. Weisstein. Geometric series. <http://mathworld.wolfram.com/GeometricSeries.html>. Accessed 01/04/2015.

A DERIVATION OF THE RISK OF ATRIAL FIBRILLATION

In order to quantify the probability of finding a non-critical defective cell, the probability of finding the first vertical couple to the right of a defective cell at a given distance must be evaluated.

Defining the probability that a cell has no transverse couples as p_ν , the probability that a cell has at least one becomes $(1 - p_\nu)$. The probability of finding the first vertical couple to the right of a defective cell at distance l_i is then:

$$p_\nu(1 - p_\nu)^{l_i} \quad (\text{A.1})$$

This is to account for having no vertical couples for l_i cells and having one vertical couple at the end.

Summing over all probabilities where $l_i < \frac{\lambda}{2}$ gives the probability that a given defective cell is non-critical.

$$P(l_i < \frac{\lambda}{2}) = \sum_{l_i=0}^{\frac{\lambda}{2}-1} p_\nu(1 - p_\nu)^{l_i} \quad (\text{A.2})$$

This is a simple geometric series sum with a known solution: $\sum_{k=0}^n ar^k = a \frac{1 - r^{n+1}}{1 - r}$ [44].

$$P(l_i < \frac{\lambda}{2}) = p_\nu \frac{1 - (1 - p_\nu)^{\frac{\lambda}{2}}}{1 - (1 - p_\nu)} \quad (\text{A.3})$$

$$= 1 - (1 - p_\nu)^{\frac{\lambda}{2}} \quad (\text{A.4})$$

This describes the probability that a given defective cell is non-critical. The probability that all defective cells in a lattice are non-critical is therefore,

$$\left[1 - (1 - p_\nu)^{\frac{\lambda}{2}}\right]^{\delta L^2} \quad (\text{A.5})$$

Finally, the probability that there exists at least one critical region gives the equation for P_{risk} ,

$$P_{\text{risk}} = 1 - \left[1 - (1 - p_\nu)^{\frac{\lambda}{2}}\right]^{\delta L^2} \quad (\text{A.6})$$

A.1 HOMOGENEOUS CONDUCTION VELOCITY

In the homogeneous conduction velocity model, the wavelength is simply one timestep. Using the equation for the wavelength in chapter 4.3.1,

$$\lambda = CV \times \tau = \tau \quad (\text{A.7})$$

The risk of fibrillation is then,

$$P_{\text{risk,homo}} = 1 - \left[1 - (1 - p_\nu)^{\frac{\tau}{2}} \right]^{\delta L^2} \quad (\text{A.8})$$

SQUARE LATTICE

For a square lattice with two possible transverse couples, the probability for a given cell to have none is simply:

$$(1 - \nu)^2$$

Therefore, p_ν for a square lattice becomes:

$$p_{\nu,\text{square}} = 1 - (1 - \nu)^2 \quad (\text{A.9})$$

Inputting this into equation A.8,

$$P_{\text{risk,square}} = 1 - \left[1 - \left\{ 1 - [1 - (1 - \nu)^2] \right\}^{\frac{\tau}{2}} \right]^{\delta L^2} \quad (\text{A.10})$$

$$= 1 - \left[1 - \left\{ (1 - \nu)^2 \right\}^{\frac{\tau}{2}} \right]^{\delta L^2} \quad (\text{A.11})$$

Hence,

$$P_{\text{risk,square}} = 1 - [1 - (1 - \nu)^\tau]^{\delta L^2} \quad (\text{A.12})$$

HEXAGONAL LATTICE

Similarly for a hexagonal lattice with 4 possible transverse connections:

$$p_{\nu,\text{hex}} = 1 - (1 - \nu)^4 \quad (\text{A.13})$$

Following through for P_{risk} using equation A.8,

$$P_{\text{risk,hex}} = 1 - [1 - (1 - \nu)^{2\tau}]^{\delta L^2} \quad (\text{A.14})$$

B COMPUTATIONAL CODE

Full computational code used for this project can be found via:

<https://github.com/bethhallowell/MSci-Project>